Alma Mater Studiorum - University of Bologna

Doctor of Philosophy in

Electronics, Computer Science and Telecomunication

Cycle XXII

Simulative Investigation on the Electronic, Vibrational and Optical Properties of the $Ge_2Sb_2Te_5$ Chalcogenide

By

Thierry B. Tsafack T.

PhD Coordinator:
Prof. Paola Mello

Supervisor:
Prof. Massimo Rudan

Final Exam 2010

Field of Science: ING/INF01 Electronics

" I want to know god's mind, all the rest are details"
Albert Einstein

" I want to know my mind like the back of my hand,
all the rest is noise"
Thierry Tsafack

To my lovely mother

Keywords

Chalcogenides
Density Functional Theory
Density Functional Perturbation Theory
Drude-Lorentz expression
Kramers-Kronig Transformation
Fresnel Equations

Preface

From the greek *chalcos* which means "ore" and *gen* which means "formation", a chalcogen is an "ore former". A chalcogen is also one of the three chemical elements Sulfur S^{16}, Selenium Se^{34} or Tellurium Te^{52}. The thread running through these 3 elements is an outer shell made up of 6 electrons, therefore a chalcogen naturally seeks 2 more electrons to stabilize. An electro-positive element is either a metal or a metalloid element with few electrons in the outer shell and thus the ability to donate them to stabilize. When one or more electro-positive elements combine with at least one chalcogen for the common purpose of stability, the resulting chemical compound is a *chalcogenide*.

Unlike other chemical compounds, chalcogenide atomic arrangement can quickly and reversibly interchange between crystalline, amorphous and liquid phases. For this reason, they are also called *phase-change materials*. Additionally, chalcogenide thermal, electrical and optical properties vary pronouncedly with the atomic arrangement leading to a number of different applications in different fields.

From a thermal standpoint, it takes an energy of $\sim$ kJ to melt 1 kg of a phase change material, that means their high heat fusion allows them to absorb a huge amount of energy in a small volume at one phase and release it in another phase. As a result, they provide remarkable benefits through thermal-energy storage for heating and cooling in residential and commercial buildings [3]. This job is made easier by phase-change-material high thermal conductivity which keeps it small the temperature gradient required for

charging the storage material. The applications stretch from air conditioning to refrigerator through solar thermal cell. Moreover, the materials ability to keep the temperature close to constant over the phase change is useful for making special clothings that keep human body at a uniform temperature.
From an optical angle, chalcogenides exhibit not only a high refractive index but also a pronounced difference between crystalline's and amorphous's. This feature along with a low phonon energy made them an ideal material for optical storage devices (CD, DVD ...) and for infrared optical fibers as they also have the ability to transmit across the full range of the infrared region of the electromagnetic spectrum [4].
Electrically, in the early 1900's Alan Tower Waterman of Yale University investigating the conductivity of molybdenide (MoS_2) observes a large negative coefficient of resistance varying with temperature and a breakdown characteristic resulting from heating the device through an electric current [5]. This experiment led him to three conclusions, which are an increase in conductivity even beyond the breakdown voltage, the potential existence of the molybdenite chalcogenide in a high-resistance and a low-resistance structure, finally the structure transition generatable by heat, electric field or light. Back then, these conclusions didn't receive any scientific and technological attention.
In 1939, while the discovery of phase-change materials for information storage applications was falling into oblivion, the first electronic computer called *ABC* was built by John Vincent Atasoff and Clifford Berry based on the *Universal Computing Machine* principles laid down by Alan Turing three years earlier. Whereas the electronic part worked pretty well, the instructions and data storage task was not always well carried out by mechanical memory card-readers. Not even the magnetic core memory [6] introduced few years later was able to meet ABC requirements thus anticipating the need of solid state memories. John Bardeen's invention of the transistor (1948) and Jack Kilby's invention of the integrated circuit (1958) gave birth to a much higher density integrated solid state non-volatile memory based on

a floating gate Metal Oxide Semiconductor Field Effect Transistor or flash transitor [7]. Non-volatile memory cells were invented based on the flash transistor ability to fill or empty the floating gate with charges. However, these devices required four terminals, high voltages and in general, they were rather big in size. Therefore, since 1960, the interest of scientists and engineers turned back on two terminal devices such as semiconductor oxides and chalcogenides.

The observation of a significant resistivity difference between two $As-Te-I$ glass region of stable conductivity by A. David Pearson in 1962 [8] and the detailed explanations of the operations of reversible switching in chalcogenide memory devices by Ovshinsky [9] increased the interest towards chalcogenides as devices for information storage. In the early 1970, the 256-bit phase change memory array by R. G. Neale and D. L. Nelson and the 1024-bit chip by Roy R. Shanks were never commercialized because of the enormous power consumption during the programming operations compared to competitive electrical programmable read-only memories in the same period.

Thanks to Gordon Moore who predicted the trend in the number of integrated circuits in silicon chips in 1965, rapid progress was made to shrink electronic devices on chip. The main chalcogenide flaw of excessive power consumption became an advantage over other technologies. As a matter of fact, the energy required to switch the phase change memory is directly proportional to the volume of the material and while silicon-based technologies show limitations as the device is shrunk, chalcogenide-based memories are in their optimal operation condition. In August 2006, BEA Systems introduced the first commercially available radiation-hardened phase change memory device. To present days, industry's and accademia's interest in phase change memory virtually exploded. The average number of US phase change memory patents per year moved from ~ 05 in the period $1966-1997$ to ~ 100 in the period $1998-2008$.

In the age of flash memories, Jesus tried to save me,

but there was no space left on his memory card.

Contents

Introduction

When shrunk below ~ 0.20 nm, charged-storage-based memory oxides break down because of the too high programming power, making flash memory cell unable to keep up with the electronic device down-scalability predicted by Gordon Moore's law. As resistance-storage-based memories scale down 5 times more, cycle more than a million times more, consume about a million times less power, are roughly 10 times faster either for the read or write operation, phase change memories represent a valid alternative. What makes chalcogenides ever so effective and efficient is the amorphous to crystalline resistance ratio of $\sim 10^3$ and their ability to quickly and interchangeably switch from amorphous to crystalline solid structure by Joule heat.
When in its crystalline phase ('set' or 'on' or '0' state) the current increases with the voltage up to a point where by Joule effect the atomic bonds break. The melted device is now rapidly quenched to prevent atoms from re-ordering thus keeping the device in an amorphous phase ('reset' or 'off' or '1' state). When in the amorphous phase, a very low current is observed until the voltage reaches a threshold point where the increase in current becomes more noticeable, goes back linearly and then goes up again showing a special S-shape behavior. When the melting point is reached, the atoms re-arrange themselves in the original crystalline ordered structure where the device is quenched again. This operation mode describes the way the cell is programmed. The 'read mode' instead is performed merely using a voltage value below the threshold point such that the attached high or low resistance tells the chalcogenide phase (amorphous or crystalline) and therefore the memory

cell state ('on/set' or 'off/reset')[19].

Since Ovshinsky first relevant contribution to understanding chalcogenide electrical features in the early 1960's, phase-change materials for information storage have been through several structural, electronic, optical and transport investigations. Crystalline cubic and hexagonal structures were measured [10] and calculated [11]. Different amorphous structures were proposed based upon molecular dynamic simulations [13] and EXAFS experiments [12]. S. Yamaka [14] calculated the hexagonal electronic structure through ab initio method implemented in *castep* [14]. Optical constants were measured for crystalline and amorphous phases [2]. D. Ielmini experimentally evidenced the trap-like amorphous conduction mechanism [15] and proposed a simulative transport model for the snap-back behavior [16]. Most importanly, very recently a Monte-Carlo model born out the trap assisted conduction mechanism highlighting the very strong trap density-dependence of the amorphous $Ge_2Sb_2Te_5$ I/V curve [17].

The present document furtherly improves the understanding of $Ge_2Sb_2Te_5$ chalcogenide by presenting its electronic, vibrational and optical properties for both crystalline phases. The basic ingredients for the vibrational and optical properties are the electronic ground and excited states. It is so for the vibrational properties because the phonon frequencies depend on the electronic ground state and it is so for optical properties for the optical response of the system translates into a certain number of electron transitions within and between valence and conduction states. For this reason, chapter 1 focuses on the electronic state calculation by highlighting the paramount principles of the theory of the electron density functional, by showing how the density functional theory combined with norm-conserving pseudo-potentials along with the expansion of atomic orbitals in plane waves is implemented within the code *Quantum Espresso* [27] and by presenting the electronic band diagram and density of states for the hexagonal and face-centered cubic phases. In chapter 2, the pillards of the density functional perturbation theory are presented as a better alternative to the *Frozen-Phonon* method, then the

computational aspects of the calculation will precede the phonon dispersion and spectrum discussed for both crystalline phases. Chapter 3 goes along the same lines first addressing the equations behind the experimental and calculated optical constants. In this instance, the real part $\epsilon_r(\omega)$ of tranverse dielectric function $\epsilon(\omega)$ is derived from the band structure using the Drude-Lorentz espression including Drude-type contribution. The imaginary part $\epsilon_i(\omega)$ is derived from $\epsilon_r(\omega)$ through the Kramers-Kronig transformation. The Maxwell model helped link the $\epsilon_r(\omega)$ and $\epsilon_i(\omega)$ to the refractive index $n(\omega)$ and the extinctive coefficient $k(\omega)$ as well as the absorption coefficient. The reflection $R(\omega)$ and transmission coefficients $T(\omega)$ are analytically derived from $\epsilon_i(\omega)$, $n(\omega)$ and $k(\omega)$ using the Fresnel equations. The computational aspect of the calculations are presented as well as the discussion of the results. For all chapters, the formalisms, the proofs of theorems and further readings are dealt with in the appendix.

Chapter 1

Electronic Properties

1.1 Density Functional Theory in a Nutshell

"If you don't like the answer, change the question"

Chalcogenides as well as any other speck of solid matter are quantum-mechanically pictured as a set of electrons and nuclei enclosed in a constant volume in space. It is then assumed that each particle moves in the field generated by all the other particles. In a quantum-mechanical language, this means that each particle feels a Hamiltonian that includes the all-electron ($\hat{T}_e$) and all-nucleus ($\hat{T}_n$) kinetic contribution, all interactions between particles of the same type ($\hat{V}_{ee}$ for electrons and $\hat{V}_{nn}$ for nuclei) and particles of different type ($\hat{V}_{en}$). The quantum procedure for determining electronic states goes through the following tasks:

Task 1 The choice of the Hamiltonian

$$\hat{H} = \hat{T}_e + \hat{T}_n + \hat{V}_{ee} + \hat{V}_{nn} + \hat{V}_{en} \tag{1.1}$$

Task 2 The choice of the solving method for the Shrödinger equation

$$\hat{H}\psi(\{\mathbf{r}_i\}, \{\mathbf{R}_j\}) = E\psi(\{\mathbf{r}_i\}, \{\mathbf{R}_j\}) \tag{1.2}$$

where i runs over the number of electrons and j the number of nuclei.

In late 1930, Douglas Hartree and Vladimir Fock came up with a method for determining the electronic states. Task 1 was carried out making the following assumptions:

- Because an electron is roughly 1838 times lighter than the lightest nucleus, the electronic and nuclear motions can be splitted. Mathematically, this means that the Hamiltonian in equation 1.1 narrows down to:

$$\hat{H} = \hat{H}_e + \hat{H}_n \tag{1.3}$$

where $\hat{H}_e = \hat{T}_e + \hat{V}_{ee} + \hat{V}_{nn} + \hat{V}_{en}$ and $\hat{H}_n = \hat{T}_n + \hat{V}_e$, $\hat{V}_e$ being the ground state energy of a system of interacting electrons moving in the field of fixed nuclei, whose Hamiltonian is $\hat{H}_e$. The straightforward consequence of 1.3 is

$$\psi(\mathbf{r}, \mathbf{R}) = \psi_e(\mathbf{r})\psi_n(\mathbf{R}) \tag{1.4}$$

leading to two Shrödinger equations, equation 1.5 for the electronic states and equation 1.6 for the nuclear states even though for the purpose of lattice dynamics addressed in chapter 2, nuclei are treated as classical particles because of their heavy mass.

$$\hat{H}_e\psi_e(\{\mathbf{r}_i\}) = E_e\psi_e(\{\mathbf{r}_i\}) \tag{1.5}$$

$$\hat{H}_n\psi_n(\{\mathbf{R}_j\}) = E_n\psi_n(\{\mathbf{R}_j\}) \tag{1.6}$$

This set of assumptions was first made by Max Born and Robert Oppenheimer in 1927 [18].

- The all-electron Hamiltonian $\hat{H}_e$ sums up the one-electron Hamiltonians $\hat{h}_i$ acting on single electrons thus the factorisation in equation 1.7.

$$\hat{H}_e = \sum_i^{N_e} \hat{h}_i \tag{1.7}$$

As far as Task 2 is concerned,

- The single-electron electronic states are calculated solving the Hartree-Fock equations $\hat{h}_i\varphi_i = \epsilon_i\varphi_i$ where the single-electron Hamiltonians include the kinetic term $\hat{T}_e$, the interaction with the nucleus $\hat{V}_{en}$ and the the coulomb and exchange energy $\hat{V}_{c-x}$ that takes in the effect of all other electrons on the i-th electron.

- To make sure that electrons are anti-symmetric particles (fermions), Ψ is computed combining φ_i through the Slater determinant

$$\Psi_i = \frac{1}{\sqrt{n!}} \begin{vmatrix} \varphi_1(1) & \varphi_1(2) & . & . & \varphi_1(n) \\ \varphi_2(1) & \varphi_2(2) & . & . & \varphi_2(n) \\ . & . & . & . & . \\ . & . & . & . & . \\ \varphi_n(1) & \varphi_n(2) & . & . & \varphi_n(n) \end{vmatrix}$$

Although the Hartree-Fock approach to the quest of the electronic states makes theoretically sense, its implementation meets some limitations as the system gets bigger. As a matter of fact, the Hamiltonian $\hat{H}_e$ is chosen as a functional of the wavefunction Ψ, consequently, there are as many Hartree-Fock equations as electrons in the system, which leads to a problem of $3N_e$ degrees of freedom. On top of that, the strong dependence on the set of functions which approximates the initial atomic orbital in the interactive solution of the Hartree-Fock equations makes them computationally almost unworkable for large systems.

In 1927, Thomas Llelwellyn [20] and Enrico Fermi [21] theoretically found out that in an ideal case of non interacting electrons $\hat{V}_{ee} \sim 0$, the electron kinetic energy can be viewed as a functional of the charge density $\hat{T}_e[n(\mathbf{r})]$ rather than the wavefunction as in the Hartree-Fock perspective $\hat{T}_e[\Psi(\mathbf{r})]$. It then turned out that the Hamiltonian too, can be expressed as functional of the charge density $\hat{H}[n(\mathbf{r})]$ and as a result, the total energy. The observations of the spectroscopist E. B. Wilson for which the electron density $n(\mathbf{r}) = N\int|\Psi(\mathbf{r},\mathbf{R})|^2 dr$ uniquely determines the positions and charges of the nuclei and thus trivially determines the Hamiltonian, unquestionably backed down Thomas and Fermi's theoretical intuition. The density functional theory was

ready to be translated into a mathematical language.

Walter Kohn along with Pierre Hohenberg proved that the ground state charge density $n_0(\mathbf{r})$ is sufficient to determine all properties of the system. This mind-blowing and startling forethought is summed up in the following theorems of Hohenberg and Kohn whose proves are dealt with in appendix A.1:

Theorem I For any system of interacting particles in an external potential $\hat{V}_n$, the external potential is determined uniquely, except for a constant, by the ground state particle charge density $n_0(\mathbf{r})$.

Corollary I Since the Hamiltonian is thus fully determined, except for a constant shift of the energy, it follows that the many-body wavefunctions for all states (ground and excited) are determined. Therefore, all properties of the system are completely determined given only the ground state density $n_0(\mathbf{r})$.

Theorem II A universal functional for the energy $E[n]$ in terms of the density $n(\mathbf{r})$ can be defined, valid for any external potential $\hat{V}_n$. For any particular external potential $\hat{V}_n(\mathbf{r})$, the exact ground state energy of the system is the global minimum value of this functional, and the density $n(\mathbf{r})$ that minimizes the functional is the exact ground state density $n_0(\mathbf{r})$

Corollary II The functional energy $E[n]$ alone is sufficient to determine the exact ground state energy and density. In general, excited states of the electrons must be determined by other means. Nevertheless, the thermal equilibrium properties such as specific heat are determined directly by the free-energy functional of the density.

In plain words, Hohenberg-Kohn theorems are a circle that begins with $n_0(\mathbf{r})$ which determines $\hat{H}[n_0(\mathbf{r})]$, which in turn determines the states $\Psi(\mathbf{r})$ that leads to the ground state $\Psi_0(\mathbf{r})$ through minimization of $E[n]$ and finally $\Psi_0(\mathbf{r})$ completes the circle coming back to $n_0(\mathbf{r})$. This simple change in perspective from $\hat{H}[\Psi(\mathbf{r})]$ (the Hartree-Fock approach) to $H[n(\mathbf{r})]$ translates

into a huge computational shift from a problem of $3N_e$ degrees of freedom to a just 3 degrees of freedom. Even though the idea that all properties of a system are actually depending only on the ground state charge density $n_0(\mathbf{r})$ was disarmingly simple and attractive, Hohenberg and Kohn theorems didn't provide any practical method for the determination of $n_0(\mathbf{r})$. Whereas the functional form of the external potential $\hat{V}_{nn}$ is known, the greatest challenge lied in the exact functional form of $\hat{T}_e$ and $\hat{V}_{ee}$ for the interacting many-body system.

In 1965, Walter Kohn and Lu Sham put forward that the interacting system where the functional form for $\hat{T}_e$ and $\hat{V}_{ee}$ are unknown and an auxiliary non-interacting system where $\hat{T}_e$ is given and $\hat{V}_{ee}$ sufficiently exact, share the same ground state charge density $n_0(\mathbf{r})$. $\hat{V}_{ee}$ has to be broken down into a classical Coulomb interaction energy called Hartree energy $\hat{V}_H$ which form is given, and an empirical exchange and correlation energy $\hat{V}_{x-c}$ that accounts for all quantum effects resulting from electron-electron interaction (electron hole interaction, exchange interaction, correlation interaction ...).

To sum it up, the density functional approach to the determination of the electronic states (both ground and excited) performs Task 1 of the quantum procedure

- Assuming the Born-Oppenheimer approximation,
- Assuming that the ground state charge density $n_0(\mathbf{r})$ is enough to determine $\hat{H}[n_0^{int}(\mathbf{r})]$ (Hohenberg-Kohn Theorems),
- Assuming the Kohn and Sham *ansatz*, i.e,

$$\begin{aligned} H[n_0^{int}(\mathbf{r})] &= H[n_0^{n-int}(\mathbf{r})] \\ &= \hat{T}_e^{n-int}[n] + \hat{V}_{nn} + \hat{V}_{en} + \hat{V}_H + \hat{V}_{x-c} \end{aligned} \tag{1.8}$$

  where $\hat{T}_e^{n-int}[n]$ is the electron kinetic energy for the non-interacting system, $\hat{V}_{nn} + \hat{V}_{en}$ is the external potential due to nucleus-nucleus interactions and electron-nucleus interaction and finally $\hat{V}_H + \hat{V}_{x-c}$ is the

electron-electron energy including the classical electron-electron repulsion and all the quantum effect associated with it.

Task 2 is carried out,

- Solving the Kohn-Sham variational equations (see appendix A.2 for the derivation of the Kohn-Sham equations)

$$\begin{aligned}[\hat{T}_e^{n-int} + \hat{V}_{nn} + \hat{V}_{en} + \hat{V}_H + \hat{V}_{x-c}]\Psi_i(\mathbf{r}) &= \epsilon_i \Psi_i(\mathbf{r}) \\ n(\mathbf{r}) &= 2\sum_i^{N_e} |\Psi_i(\mathbf{r})|^2. \quad (1.9)\end{aligned}$$

From a pragmatic vantage point, the theoretical nutshell of the density-functional theory is the Hohenberg-Kohn theorems and its computational nutshell is the Kohn-Sham variational equations. For this reason, the next chapter focuses on how to feed equations 1.9 into a computer to get the $Ge_2Sb_2Te_5$ electronic states for both crystalline phases.

1.2 Density Functional Theory in a Computer

"To err is human, but to really foul things up requires a computer"

In this chapter, we focus on how to make the theory of the density functional the most practical for the electronic state calculations. There are two possible ways to find the electronic states assuming fixed atomic positions. The first is to solve self-consistently the Kohn-Sham equations 1.9 by diagonalizing the Hamiltonian matrix and iterating on the charge density (or the potential) until self-consistency is achieved. The second is to directly minimize the energy functional as a function of the coefficients of Kohn-Sham orbitals in the plane waves (or other) basis set, under the constraint of orthonormality for Kohn-Sham orbitals. The basic ingredients are in both cases the same. The first approach is used here. Hence, the reason behind what follows is three-fold. Underline the conceptual assumptions as well as the numerical approximations to the Kohn-Sham equations, lay out the steps of

the calculations which are structural optimisation, self and non-self consistent calculations and finally discuss the pros and cons of the approximations mainly showing how and why they negatively impact the accuracy of the band gap.

1.2.1 Conceptual and Numerical Approximations

The first equation of 1.9 cannot be fully solved without introducing some assumptions on each term. Here they are,

- The kinetic term for the auxiliary non-interacting system is chosen to be non-relativistic and spinless

$$\hat{T}_e^{n-int} = -\frac{\hbar}{2m}\nabla^2 \tag{1.10}$$

- Because the core electrons are electrostatically bound to the nuclei, they too, as well as the nuclei do not contribute significantly to the electronic properties. Thence, each atom can be safely replaced by a pseudo-atom that incorporates the nucleus and its core electrons into a *pseudo-nucleus* and let outer electrons be exclusively responsible for the electronic properties. The pseudo-system made up of pseudo-atoms has an external potential called *pseudopotential*

$$\hat{V}_n^{ps} \longleftarrow \hat{V}_n + \text{core electrons} \tag{1.11}$$

  that substitutes the second and third terms of equation 1.9 (see appendix A.3 for the proof of the validity of pseudo-potential approximation). To make sure that the pseudo-system doesn't change relevantly the electronic properties, the pseudopotential $\hat{V}_n^{ps}$ is built such that all-electron wavefunctions and pseudo-wavefunctions have the same energy, they match beyond a core radius and the resulting charge density has to coincide within the same core radius. Such a pseudopotential is named *norm-conserving* pseudopotential.

- The fourth term in 1.9 is the Hartree potential given by equation A.21.

- The fifth term of 1.9 is the exchange and correlation potential defined in equation A.22 where the dependence on the exchange and correlation energy is self-evident. In their original paper (1965), Kohn and Sham suggested the assumption that each small volume of the system (so small that the charge density can be thought to be constant therein) contributes the same exchange-correlation energy as an equal volume of a homogeneous electron gas at the same density. With this assumption, the exchange-correlation energy functional and potential reads

$$E_{x-c} = \int \epsilon_{x-c}(n(\mathbf{r}))n(\mathbf{r})d\mathbf{r} \tag{1.12}$$

  which through A.22 leads to

$$\hat{V}_{x-c} = \epsilon_{x-c}(n(\mathbf{r})) + n(\mathbf{r})\frac{\partial\epsilon_{x-c}(n(\mathbf{r}))}{\partial n(\mathbf{r}))} \tag{1.13}$$

  where $\epsilon_{x-c}(n(\mathbf{r}))$ is the exchange-correlation energy per particle in an homogeneous electron gas at density $n(\mathbf{r})$. This approximation is known as the *local density approximation* (LDA). The approximate form of $\epsilon_{x-c}(n(\mathbf{r}))$ is calculated using Monte-Carlo simulations for the homogeneous electron gas.

- The one-electron wavefunction in equation 1.9 is approximated using a plane wave basis set

$$\Psi_i(\mathbf{r}) = \frac{1}{\Omega}c_{\mathbf{k},\mathbf{G}}e^{i(\mathbf{k}+\mathbf{G})\mathbf{r}} \tag{1.14}$$

  where Ω is the crystal volume, $\mathbf{k}$ is a Bloch vector in the Brillouin Zone and $\mathbf{G}$ is a reciprocal lattice vector. Geometrically, the plane waves in 1.14 can be thought as a grid in the $\mathbf{k}$-space. Ideally, that expansion is infinite, but computationally, it has to be truncated because the contribution from higher Fourier components (large $|\mathbf{k}+\mathbf{G}|$) is small. This takes place by setting the cut off energy E_{cut} such that

$$\frac{\hbar^2|\mathbf{k}+\mathbf{G}|^2}{2m} \leq E_{cut} \tag{1.15}$$

Plugging 1.14 into the first equation in 1.9 we get

$$\sum_{\mathbf{G}'} H_{\mathbf{k+G},\mathbf{k+G}'} c_{i,\mathbf{k+G}'} = \epsilon_i c_{i,\mathbf{k+G}} \tag{1.16}$$

where the matrix elements are

$$H_{\mathbf{k+G},\mathbf{k+G}'} = \frac{1}{2}|\mathbf{k}+\mathbf{G}|^2 + V_n^{ps}(\mathbf{k}+\mathbf{G},\mathbf{k}+\mathbf{G}') + V_H(\mathbf{G}-\mathbf{G}') + V_{x-c}(\mathbf{G}-\mathbf{G}') \tag{1.17}$$

the pseudo-nuclei potential is defined as

$$V_n^{ps}(\mathbf{G}) = \sum_{\alpha} S_\alpha(\mathbf{G}) v_\alpha(\mathbf{G}) \tag{1.18}$$

with

$$S_\alpha(\mathbf{G}) = \sum_{I} e^{i\mathbf{G}\mathbf{R_I}}. \tag{1.19}$$

Solving equation 1.16 goes through the diagonalization of the matrix whose elements are given in 1.17. Such an operation is the most computationally demanding process of the entire electronic properties calculation. In fact, $N_{PW} > 100 \times$ number of atoms in the unit cell being the number of plane waves, it takes about N_{PW}^2 elements to be stored and the computational time to diagonalize a $N_{PW} \times N_{PW}$ matrix grows as N_{PW}^3.
As far as the charge density is concerned, one has to sum over an infinite number of **k**-points, thus the second equation of 1.9 turns into

$$n(\mathbf{r}) = \sum_{\mathbf{k}} \sum_{i} |\Psi_i(\mathbf{r})|^2 \tag{1.20}$$

where the index i runs over occupied bands. Assuming periodic (Born-Von Karman) boundary conditions

$$\Psi_i(\mathbf{r}+L_1\mathbf{R}_1) = \Psi_i(\mathbf{r}+L_2\mathbf{R}_2) = \Psi_i(\mathbf{r}+L_3\mathbf{R}_3) = \Psi_i(\mathbf{r}) \tag{1.21}$$

with $L = L_1L_2L_3$ being the number of allowed **k**-points as well as the number of unit cells. In the "thermodynamic" limit of an infinite crystal, $L \longrightarrow \infty$, the sum over **k** becomes an integral over the Brillouin Zone. Experience shows that this integral can be approximated by a discrete sum over an affordable

number of **k**-points, at least in insulators and semiconductors. When present, symmetry can be used to further reduce the number of calculations to be performed. Only one **k**-point is left to represent each *star* (the set of **k**-points that are equivalent by symmetry) with a weight ω_i that is proportional to the number of **k**-points in the star. The infinite sum over the Brillouin Zone is replaced by a discrete sum over a set of points $\mathbf{k}_i$ and weights ω_i:

$$\frac{1}{L}\sum_{\mathbf{k}} f_{\mathbf{k}}(\mathbf{r}) \longrightarrow \sum_{i} \omega_i f_{\mathbf{ki}}(\mathbf{r}). \tag{1.22}$$

The resulting sum is then symmetrized to get the charge density.
The above approximations and comments being made, we are ready to address the actual electronic property calculations through the solution of 1.16 coupled with 1.20 where the unknowns are the coefficients of the expansion in plane waves $c_{\mathbf{k},\mathbf{G}}$ and the eigenvalues ϵ_i.

1.2.2 Computational Steps

At this point, it is instrumental to recall that the density functional theory is a ground state theory which assumes the Born-Oppenheimer approximation. Within such an approximation, the separabillity of the electron-nucleus Hamiltonian 1.3 into an electron Hamiltonian and a nuclei Hamiltonian with all that comes with it (see equation 1.4), rests on the fact that the valence electrons are supposed to move in a field of fixed pseudo-nuclei. This seemingly harmless statement contains all the steps of our calculation. It stands to reason that the foremost requirement to be met is to keep the pseudo-nuclei fixed. The procedure that meets this condition is called *structural relaxation* and is the first step toward the electronic states, then self-consistent solution of the Kohn-Sham equations leads to the electronic ground state wheras the excited states are obtained solving the same equations non self-consistently.

Structural Relaxation

As stated earlier, structural optimisation involves keeping the pseudo-nuclei fixed, but the resulting structure wouldn't be in its ground state if the lattice

parameters didn't match the ground state energy. Therefore, it is foundational to see the ground state energy as a functional of both cell parameters and atomic positions. Since pseudo-nuclei are way heavier than valence electrons, they can be treated as classical particles, therefore solving 1.6 wouldn't be appropriate. It is safer to rely on the second law of dynamics, hence to keep the pseudo-nuclei fixed means having the force F_{ps-n} acting on them to abide by

$$F_{ps-n} = -\nabla E(B_\beta, \mathbf{R}_{\beta\alpha}) = 0 \Rightarrow \frac{\partial E(B_\beta, \mathbf{R}_{\beta\alpha})}{\partial B_\beta \partial \mathbf{R}_{\beta\alpha}} = 0 \tag{1.23}$$

and

$$\frac{\partial^2 E(B_\beta, \mathbf{R}_{\beta\alpha})}{\partial {B_\beta}^2 \partial {\mathbf{R}_{\beta\alpha}}^2} > 0 \tag{1.24}$$

where $B_\beta \equiv a_i, b_j, c_k$ the physical box for the lattice cell whose sides are a_i, b_j, c_k whereof any combination of subscript i, j and k leads to a different box with suscript β. $\mathbf{R}_{\beta\alpha}$ is the pseudo-nucleus positions within the box B_β. $E(B_\beta, \mathbf{R}_{\beta\alpha})$ is the valence electron ground state energy. Structural optimisation is thus referred to as the process whereby we choose the particular box B_0 and the nucleus positions $\mathbf{R}_{00}$ within B_0 that minimizes the ground state energy $E(B_\beta, \mathbf{R}_{\beta\alpha})$. This process breaks into two steps

Task A For each box B_β with $\beta \equiv i, j, k$ running from 1 to n, every set of pseudo-nucleus positions $\mathbf{R}_{\beta\alpha}$ with α spanning from 1 to m leads to m different energy $E_{\beta\alpha}$. The minimum of all m $E_{\beta\alpha}$ is the minimum energy for the box α, $E_{\beta 0}$. The purpose of this step is to find $\mathbf{R}_{\beta 0}$ out of all the m $\mathbf{R}_{\beta\alpha}$ that leads to $E_{\beta 0}$.

Task B Out of all the n boxes B_β with $E_{\beta 0}$, the box with the minimum $E_{\beta 0}$ is B_0, the box with the minimum energy E_{00}. The combination of box B_0 and the nucleus positions $\mathbf{R}_{00}$ is the geometry that minimizes the energy. What's more, the combination of box B_0 and the nucleus positions $\mathbf{R}_{00}$ is the structure that meets the Born-Oppenheimer approximation. Finally, that combination of box B_0 and the nucleus positions $\mathbf{R}_{00}$ is the relaxed structure that keeps pseudo-nuclei still while valence electrons gravitate around them.

Task **A** and **B** can be computed either manually or using a *variable cell molecular dynamics* approach [22]. In either way, the structural relaxation procedure is the most computationally demanding process in electronic property calculations.

Finding the Ground States

The lattice parameters along with the fixed pseudo-nucleus positions resulting from the structural optimisation being known, equations 1.16 and 1.20 can be solved to find ground state charge density and therefore the ground state eigenfunctions and eigenvalues. According to the Hohenger-Kohn theorems, a starting charge $n_{in}(\mathbf{r})$ uniquely determines the Hamiltonian which through 1.16 determines the wavefunctions which in turn determine through 1.20 a new charge density $n_{out}(\mathbf{r})$. The consecutive application of equations 1.16 and 1.20 can be combined into the functional **A** such that

$$n_{out}(\mathbf{r}) = \mathbf{A}[n_{in}(\mathbf{r})]. \tag{1.25}$$

We know that the ground state charge density meets the requirement

$$n(\mathbf{r}) = \mathbf{A}[n(\mathbf{r})]. \tag{1.26}$$

The most intuitive and straightforward approach is to use $n_{out}(\mathbf{r})$ as the new input charge density

$$n_{in}^{(i+1)} = n_{out}^{(i)} \tag{1.27}$$

where the superscripts are the iteration numbers. Unfortunately, there is no guarantee that this will work, and experience shows that it usually does not. The reason is that the algorithm will work only if the error on the out-density is smaller than the corresponding error on the in-density. An in-density error $\delta n_{in}(\mathbf{r})$, leads at self-consistency to an out-density error along the lines of

$$\delta n_{out}(\mathbf{r}) \simeq \int \frac{\delta \mathbf{A}}{\delta n(\mathbf{r})} \delta n_{in}(\mathbf{r}) d\mathbf{r} \equiv \mathbf{J}\delta n_{in} \tag{1.28}$$

which may or may not be smaller than the in-density error, depending on the size of the largest eigenvalue, $e_{\mathbf{J}}$, of the operator **J**, which is related to

the dielectric response of the system. Usually, $e_{\mathbf{J}} > 1$ and the iteration does not converge.
A simple algorithm that generally works, although sometimes slowly, is the *simple mixing*. A new input charge density is generated by mixing the in and out charge densities

$$n_{in}^{(i+1)} = (1-\alpha)n_{in}^{(i)} + \alpha n_{out}^{(i)} \tag{1.29}$$

The value of α must be chosen empirically in order to speed the convergence up. The error with respect to self-consistency becomes

$$\delta n_{out} = [(1-\alpha) + \alpha \mathbf{J}]\delta n_{in} \tag{1.30}$$

and it can be easily proven that the iteration converges if $\alpha < |\frac{1}{e_{\mathbf{J}}}|$. Doing so, the ground state charge density provides the ground state wavefunctions and energies.

Finding the Excited States

As a consequence of the Hohenberg-Kohn theorems, any charge density corresponding to any other minima/maxima but the absolute minima of the energy functional, leads to an excited state of the system. As a result, contrarily to the self-consistent procedure used for determining the ground states, the excited states can be easily computed solving equations 1.16 and 1.20 non self-consistently.

1.2.3 Successes and Failures of DFT

The calculation of electronic properties through the density functional theory has strengths and weaknesses depending on the system under investigation. Its attractiveness lies in cutting by N_e the degrees of freedom of the equations behind the calculations reducing very significantly the computational load attached to them. On top of that, the expansion of wavefunctions in a plane wave basis set goes hand in hand with the periodicity of the crystal thus furtherly decreases the computational load than if localized basis set was

used.

Conversely, this comfortable computability comes with some approximations which cannot help but curb the accuracy the results. The most impacting approximation on the electronic properties is the local density approximation which overestimates ($\sim 20\%$ and more) cohesive energies and bond strengths in molecules and solids. For the purpose of our calculations, the most rilevant problem associated with it is the miscalculation of the band gap addressed in the following lines.

Local Density Approximation and the Band Gap

If one electron in the state v is removed from the system, $E_N - E_{N-1} = \epsilon_v$, where E_N is the energy of the system with N electrons. Likewise, an addition of an electron in the state c leads to $E_{N+1} - E_N = \epsilon_c$. The difference between the largest addition energy and the smallest removal energy defines the energy band gap

$$E_g = \epsilon_c - \epsilon_v = E_{N+1} - E_{N-1} - 2E_N. \tag{1.31}$$

In solids, this is the onset of the continuum of optical transitions, if the gap is direct (if the lowest empty state and the highest filled state have the same k vector). From atomic and molecular physics, the highest occupied and lowest unoccupied states are respectively called HOMO (Highest Occupied Molecular Orbital) and LUMO (Lowest Unoccupied MO), while addition and removal energy are respectively referred to as *electron affinity*, **A**, and *ionization potential*, **I**. Due to the discontinuity of exchange-correlation potential (see the discussion in appendix A.4), it is safe to say, $E_g = \mathbf{I} - \mathbf{A}$ which in turn can be written as

$$\begin{aligned} E_g &= -\mu(N-\delta) + \mu(N-\delta) \\ &= \left.\frac{\delta E}{\delta n(\mathbf{r})}\right|_{N+\delta} - \left.\frac{\delta E}{\delta n(\mathbf{r})}\right|_{N-\delta} \end{aligned} \tag{1.32}$$

with $\delta \longrightarrow 0$.

Substituting to $E[n(\mathbf{r})]$ the explicit Kohn-Sham form in A.14. The Hartree

and external potential terms of the functional will yield no discontinuity and no contribution to E_g. Only the kinetic and exchange-correlation terms may have a discontinuity and contribute to E_g.
For a non interacting system, only the kinetic term contributes, and the gap is exactly given by the auxiliary non interacting system gap:

$$\begin{aligned} E_g^{n-int} &= \left.\frac{\delta T_{n-int}}{\delta n(\mathbf{r})}\right|_{N+\delta} - \left.\frac{\delta T_{n-int}}{\delta n(\mathbf{r})}\right|_{N-\delta} \\ &= \epsilon_{LUMO} - \epsilon_{HOMO} \end{aligned} \tag{1.33}$$

It is remarked that even the kinetic energy of non interacting electrons, considered as a functional of the density, must have a discontinuous derivative when crossing an integer number of electrons. This is one reason why it is so difficult to produce explicit functionals of the charge density for T_{n-int} that are able to yield good results: no simple functional form will yield the discontinuity, but this is needed in order to get the correct energy spectrum.
For the interacting system:

$$\begin{aligned} E_g &= \left.\frac{\delta T_{n-int}}{\delta n(\mathbf{r})}\right|_{N+\delta} - \left.\frac{\delta T_{n-int}}{\delta n(\mathbf{r})}\right|_{N-\delta} + \left.\frac{\delta E_{x-c}}{\delta n(\mathbf{r})}\right|_{N+\delta} - \left.\frac{\delta E_{x-c}}{\delta n(\mathbf{r})}\right|_{N-\delta} \\ &= E_g^{n-int} + E_g^{x-c} \end{aligned} \tag{1.34}$$

Note that the kinetic term is evaluated at the same charge density as for the non interacting system, so it coincides with the auxiliary non interacting system gap.
By virtue of 1.34 the gaps calculated through the density functional theory are not by construction equal to the true gap because they are missing a term (E_g^{x-c}) coming from the discontinuity of derivatives of the exchange-correlation functional. This is absent by construction from any current approximated functional (be it LDA or gradient-corrected or more complex). There is some evidence that this missing term is responsible for a large part of the band gap problem, at least in common semiconductors.

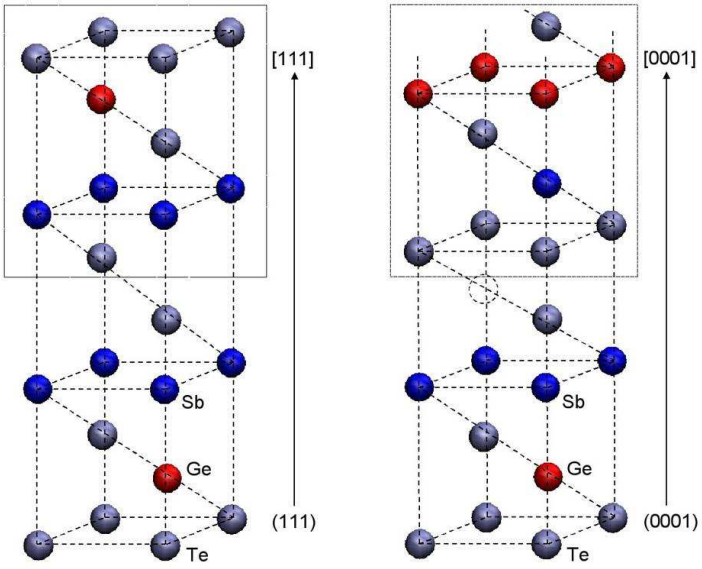

Figure 1.1: Atomic arrangement of the hexagonal (left) and of the fcc (right) GST, showing the stacking sequence along the crystalline planes shown.

1.3 Results and Discussion

In this section, we present the parameters used in the electronic property calculations as well as the band structure and the density of states for both chalcogenide phases.

The starting lattice parameters and atomic positions for the structure relaxation are taken from experiments [10]. The hexagonal experimental structure is made up of 9 atoms in the hexagonal unit cell arranged in the stacking sequence $Te - Ge - Te - Sb - Te - Te - Sb - Te - Ge$. The FCC experimental structure results from hexagonal's shifting $Te - Sb - Te - Ge$ sub-unit along the [210] direction thus creating a vacancy site leading to unit cell of 27 atoms and 3 vacancies arranged in the stacking sequence $Te - Ge - Te - Sb - Te - v - Te - Sb - Te - Ge$ repeated three times (see figure 1.1). The whole relaxation process for the hexagonal structure took around 2 days on a 8-processor Linux cluster. Due to its intrinsic greater structural complexity, the computational load of the FCC cell proved to be 4 times higher. The structure optimisation resulted in a cell parameter de-

viation from the experimental data of $\Delta a = 0.08\%$, $\Delta c = 3.02\%$ for the hexagonal phase and $\Delta a = -1.19\%$, $\Delta c = 0.11\%$ for the FCC cubic phase. The self (ground states) and non self-consistent (the excited states) calculations were carried out using the Perdew and Zunger exchange-correlation energy [27] along with the non-conserving ionic Bachelet-Hamann-Schluter pseudopotentials [27] (as for the electron-ion interaction), a cut off energy of 80 Ryd and the following valence configurations $4s^2 4p^2$, $5s^2 5p^3$, and $5s^2 5p^4$ for Ge, Sb, and Te, respectively. The mixing parameter for the charge density convergence in equation 1.30 is set to be 0.3 for both phases. By the same token, the convergence threshold on the total energy was set to be 10^{-7} for both phases.

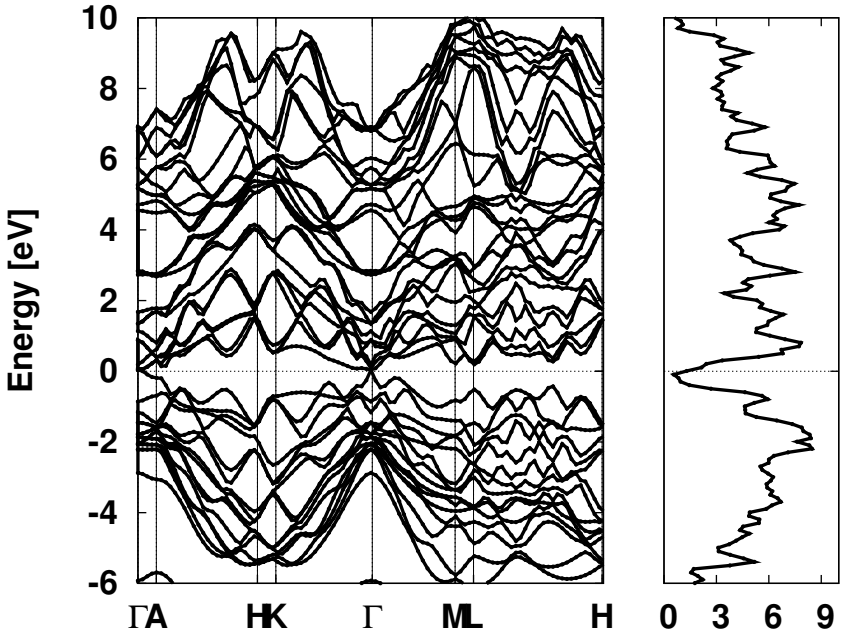

Figure 1.2: Hexagonal band diagram along the high symmetry lines (left) and density of states (right).

The hexagonal electronic structure along the high symmetry lines in figure 1.2 shows no band gap wheras the FCC band structure along the same high symmetry lines in figure 1.3 exhibits a band gap of about 0.1 eV. Both values of the band gap are not in agreement with the experimental ones (0.5 eV) for

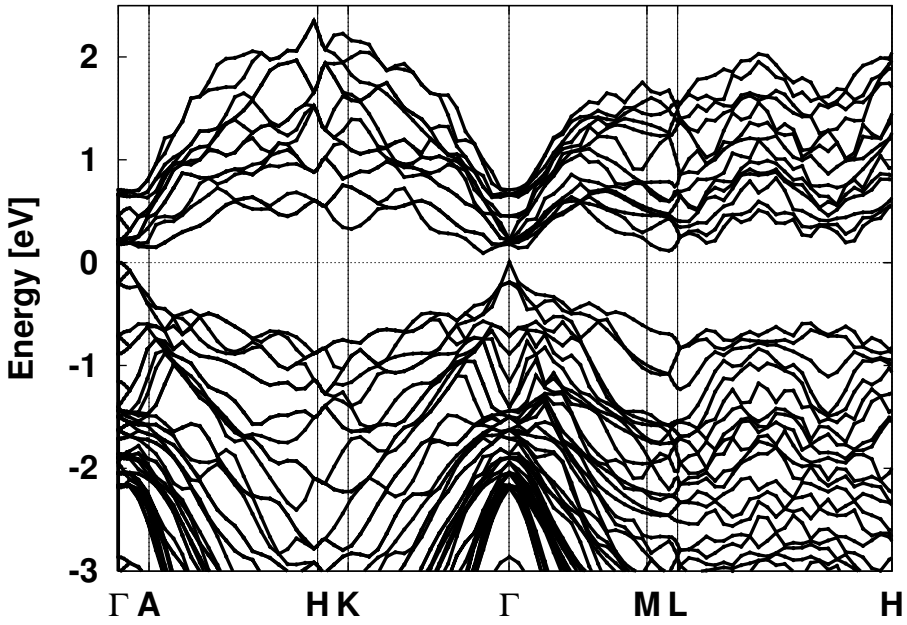

Figure 1.3: FCC band diagram along the high symmetry lines.

the reasons laid out in the previous section. It should be pointed out that the band gap increase from hexagonal to FCC is mainly due to the increase of defects in the structure therefore we would expect the amorphous $Ge_2Sb_2Te_5$ band gap to be even higher because of a larger number of vacancy sites. This is supported also by the amorphous experimental band gap ~ 0.7 eV larger than the crystalline one (~ 0.5 eV). What's more, a direct band gap observed in figure 1.2 and an indirect band gad observed in figure 1.3 are confirmed by optical experiments [2]. We will elaborate on that in the section dedicated to optical properties. The FCC density of states compared to the experimental one [23] in figure 1.4 shows a good matching as it relates to the valence band states.

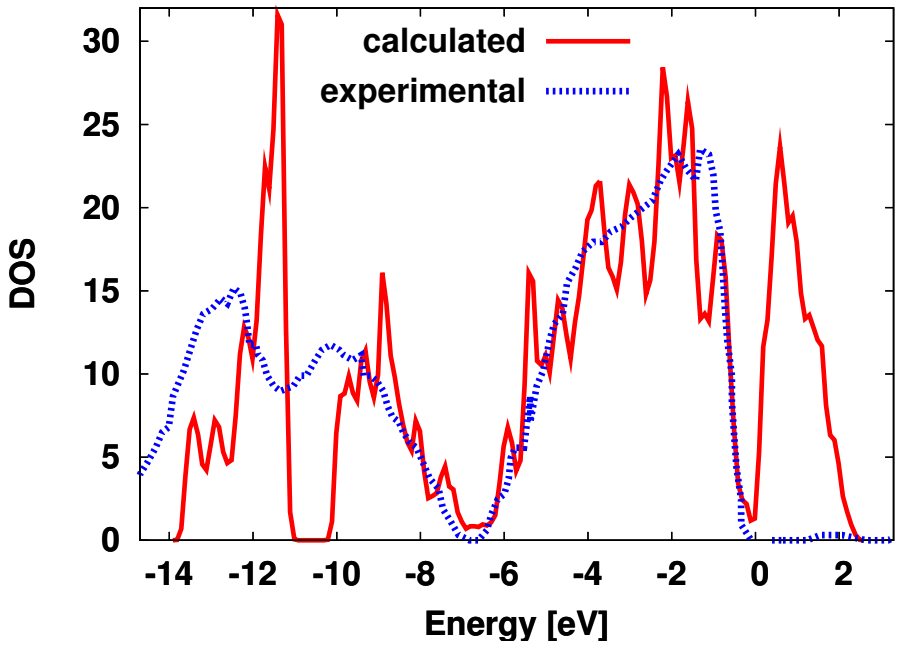

Figure 1.4: Calculated (solid line) and experimental (dashed line) FCC density of states.

Chapter 2

Vibrational Properties

In this section, the phonon calculation is addressed. The equation behind the nuclear motion is derived and shows a dependence on the second derivative of the total energy. Unlike the *frozen phonon* approach which diretly computes the second derivative of the total energy as a function of the nucleus positions, the perturbative approach computes the same quantity viewing it as a functional of the ground state electron density and its linear response. The latter is calculated within the density-functional perturbation theory whose principles are shown in the first section. DFPT's and phonon's implementation are shown in the second section.

2.1 Phonons and the Density Functional Perturbation Theory in a Nutshell

2.1.1 Phonons

The Shrödinger equation for nuclei in 1.6 would hold if their motion were as fast as electrons'. Since nuclei are way heavier, their motion is way slower. It is thus safe to treat them as classical particles. Whereas the net force acting on each nucleus has to vanish to keep it fixed at its equilibrium positions

(1.23), the following condition is required to calculate their motion

$$M_n \frac{\partial^2 \mathbf{R}_n}{\partial t^2} = \mathbf{F}_n(\mathbf{R}) = -\frac{\partial}{\partial \mathbf{R}_n} E(\mathbf{R}_n) \tag{2.1}$$

where $E(\mathbf{R}_n)$ is the ground state energy $\mathbf{R}_n$, M_n is the nucleus mass, and $\mathbf{R}_n(t)$ is the motion of each nuclear position. Within the *harmonic approximation* [24] the nuclear motion is thought of as a vibrational mode at frequency ω and described by displacements

$$\mathbf{u}_n(t) = \mathbf{R}_n(t) - \mathbf{R}_n^{eq} \simeq \mathbf{u}_n e^{i\omega t} \tag{2.2}$$

where $\mathbf{R}_n^{eq}$ is the nuclei position such that $\mathbf{F_n}(\mathbf{R_n^{eq}}) = \mathbf{0}$.
Expanding $E(\mathbf{R}_n)$ in power of displacements we get

$$E = E_0 + C_{n_i}^{\alpha} \mathbf{u}_{n_i} + C_{n_i n_j}^{\alpha\beta} \mathbf{u}_{n_i} \mathbf{u}_{n_j} + ... \tag{2.3}$$

where the coefficients of the expansion are called *interatomic force constants* and defined as

$$\begin{aligned} C_{n_i}^{\alpha} &= \frac{\partial E(\mathbf{R}_n)}{\partial \mathbf{R}_{n_i}^{\alpha}} \\ C_{n_i n_j}^{\alpha\beta} &= \frac{\partial^2 E(\mathbf{R}_n)}{\partial \mathbf{R}_{n_i}^{\alpha} \partial \mathbf{R}_{n_j}^{\beta}} \\ &\vdots \end{aligned} \tag{2.4}$$

Knowing that $C_{n_i}^{\alpha} = 0$ because of 1.23 and leaving out all the terms of the expansion from the third, 2.3 and 2.2 into 2.1 leads to

$$-\omega^2 M_{n_i} u_{n_i}^{\alpha} = -\sum_{n_j \beta} C_{n_i n_j}^{\alpha\beta} u_{n_j}^{\beta} \tag{2.5}$$

for each i-th nucleus. The full solution for all vibrational states is a set of independent oscillators with each vibrational frequency ω, determined by the secular equation,

$$\det \left| \frac{1}{\sqrt{M_{n_i} M_{n_j}}} C_{n_i n_j}^{\alpha\beta} u_{n_j}^{\beta} - \omega^2 \right| = 0 \tag{2.6}$$

where the dependence upon masses M_{n_i}, M_{n_j} has been cast in symmetric form. The problem in solving 2.6 comes down to how to calculate

$$C_{n_i n_j} = \frac{\partial^2 E(\mathbf{R}_n)}{\partial \mathbf{R}_{n_i} \partial \mathbf{R}_{n_j}} \tag{2.7}$$

where the super-scripts α and β were dropped down for sake of simplicity. While the frozen phonon approach calculates 2.7 computing the total energy as a function of $\mathbf{R}$, we use the DFT perspective that views the total energy as a functional of the charge density $n(\mathbf{r})$. The Hellmann-Feynman theorem [28] is used. It states that

$$\mathbf{F}_{n_i} = -\int n(\mathbf{r}) \frac{\partial V_{en}}{\partial \mathbf{R}_{n_i}} d\mathbf{r} - \frac{\partial V_{nn}}{\partial \mathbf{R}_{n_i}} \tag{2.8}$$

where

$$\begin{aligned} V_{en} &= -\sum_{in_i} \frac{Z_{n_i} e^2}{|\mathbf{r}_i - \mathbf{R}_{n_i}|} \\ V_{nn} &= \frac{e^2}{2} \sum_{n_i \neq n_j} \frac{Z_{n_i} Z_{n_j}}{|\mathbf{R}_{n_i} - \mathbf{R}_{n_j}|} \end{aligned} \tag{2.9}$$

are the electron-nucleus and the nucleus-nucleus potentials respectively. The second derivative of appearing in 2.7 is then calculated making use of 2.8 leading to

$$\begin{aligned} \frac{\partial^2 E(\mathbf{R}_n)}{\partial \mathbf{R}_{n_i} \partial \mathbf{R}_{n_j}} &= \frac{\partial \mathbf{F}_{n_i}}{\partial \mathbf{R}_{n_j}} \\ &= \int \frac{\partial n(\mathbf{r})}{\partial \mathbf{R}_{n_j}} \frac{\partial V_{en}}{\partial \mathbf{R}_{n_i}} d\mathbf{r} + \int n(\mathbf{r}) \frac{\partial^2 V_{en}(\mathbf{r})}{\partial \mathbf{R}_{n_i} \partial \mathbf{R}_{n_j}} d\mathbf{r} + \frac{\partial^2 V_{nn}(\mathbf{r})}{\partial \mathbf{R}_{n_i} \partial \mathbf{R}_{n_j}} \end{aligned} \tag{2.10}$$

It is worth noting in equation 2.10 that the matrix of inter-atomic force constants rests on the ground state electron charge density, $n(\mathbf{r})$ and its linear response to a distortion of the nuclear geometry $\partial n(\mathbf{r})/\partial \mathbf{R}_{n_j}$. While the former is calculated solving self-consistently equations 1.9, the latter is calculated resorting to the theory of the density functional perturbation.

2.1.2 Density Functional Perturbation Theory

In the following, the change of parameter from $\mathbf{R}_{n_i}$ to $\lambda \equiv \{\lambda_i\}$ is made to simplify the notation. According to the Hellmann-Feynman theorem, the first and second derivatives of the ground-state energy can be written as

$$\frac{\partial E}{\partial \lambda_i} = \int \frac{\partial V}{\partial \lambda_j} n(\mathbf{r}) d\mathbf{r} \tag{2.11}$$

$$\frac{\partial^2 E}{\partial \lambda_i \partial \lambda_j} = \int \frac{\partial^2 V_n}{\partial \lambda_i \partial \lambda_j} n(\mathbf{r}) d\mathbf{r} + \int \frac{\partial n(\mathbf{r})}{\partial \lambda_i} \frac{\partial V_n}{\partial \lambda_j} n(\mathbf{r}) d\mathbf{r} \tag{2.12}$$

The electron-density response, $\partial n(\mathbf{r})/\partial \lambda_i$, in 2.11 can be evaluated linearizing the Kohn-Sham equations 1.9 with respect to wave-function, density, and potential variations. The linearization of the charge density equation in 1.9 leads to:

$$\Delta n(\mathbf{r}) = 4\Re \sum_{n=1}^{\frac{N}{2}} \Psi_n(\mathbf{r}) \Delta \Psi_n(\mathbf{r}) \tag{2.13}$$

where the finite-difference operator Δ^λ is defined as:

$$\Delta^\lambda F = \sum_i \frac{\partial F}{\partial \lambda_i} \Delta \lambda_i \tag{2.14}$$

Since the external potential (both unperturbed and perturbed) is real, each Kohn-Sham eigenfunction and its complex conjugate are degenerate. As a consequence, the imaginary part of the sum in 2.13 vanishes, so that the prescription to keep only the real part can be dropped.
The variation of the KS orbitals, $\Delta\Psi_n(n(\mathbf{r}))$, is obtained by standard first-order perturbation theory [25]

$$(H_{SCF} - \epsilon_n)|\Delta\Psi_n\rangle = -(\Delta V_{SCF} - \Delta\epsilon_n)|\Psi_n\rangle \tag{2.15}$$

With

$$H_{SCF} = -\frac{\hbar^2}{2m}\frac{\partial^2}{\partial \mathbf{r}^2} + V_{SCF}(\mathbf{r}) \tag{2.16}$$

being the unperturbed KS Hamiltonian and

$$\Delta V_{SCF}(\mathbf{r}) = \Delta V(\mathbf{r}) + e^2 \int \frac{\Delta n(\mathbf{r}')}{|\mathbf{r} - \mathbf{r}'|} d\mathbf{r}' + \left.\frac{dv_{x-c}}{dn}\right|_{n=n(\mathbf{r})} \Delta n(\mathbf{r}) \tag{2.17}$$

the first-order correction to the self-consistent potential. $\delta\epsilon_n = \langle\Psi_n|\Delta V_{SCF}|\Psi_n\rangle$ is the first order variation of the Kohn-Sham eigenvalue, ϵ_n.

Equations 2.13, 2.17 and 2.15 form a set of self-consistent equations for the perturbed system similar to the Kohn-Sham equations 1.9 in the unperturbed case. In 2.15, the self-consistency requirement manifests itself in the dependence of the right-hand side upon the solution of the linear system. As $\Delta V_{SCF}(\mathbf{r})$ is a linear functional of $\Delta n(\mathbf{r})$ which in turn depends linearly on the $\Delta\Psi$'s, the whole self-consistent calculation can be cast in terms of a generalized linear problem. It should be pointed out that though the right-hand side of 2.15 for $\Delta\Psi_n$ depends through Δn on the solution of all the similar equations holding for the $\Delta\Psi_m$, $(m \neq n)$. Therefore, all the N equations, 2.15, are linearly coupled to each other, and the set of all the $\Delta\Psi$ is the solution of a linear problem whose dimension is $(NM/2 \times NM/2)$, M being the size of the basis set used to describe the Ψ's. Whether this big linear system is better solved directly by iterative methods or by the self-consistent solution of the smaller linear systems given by 2.15 is a matter of computational strategy.

The first-order correction to a given eigen-function of the Schrödinger equation, given by 2.15, is often expressed in terms of a sum over the spectrum of the unperturbed Hamiltonian,

$$\Delta\Psi_n(\mathbf{r}) = \sum_{m\neq n} \Psi_m(\mathbf{r}) \frac{\langle\Psi_m|\Delta V_{SCF}|\Psi_n\rangle}{\epsilon_n - \epsilon_m} \tag{2.18}$$

running over all the states of the system, occupied and empty, with the exception of the state being considered, for which the energy denominator would vanish. Using Equation 2.18, the electron charge-density response in 2.13 can be cast into the form:

$$\Delta n(\mathbf{r}) = 4 \sum_{n=1}^{\frac{N}{2}} \sum_{m\neq n} \Psi_n^*(\mathbf{r}) \frac{\langle\Psi_m|\Delta V_{SCF}|\Psi_n\rangle}{\epsilon_n - \epsilon_m} \tag{2.19}$$

which shows that the contributions to the electronic density response coming from products of occupied states cancel out, so that the m index can

be thought as running onto conduction states only. This is tantamount to say that the electron density distribution does not respond to a perturbation which only acts onto the occupied-state manifold (or, more generally, to the component of any perturbation which couples occupied states among each other).

The explicit evaluation of $\Delta\Psi$ out of 2.18 would require the knowledge of the whole spectrum of the Kohn-Sham Hamiltonian and extensive summations over conduction bands. In Equation 2.15, instead, only the knowledge of the occupied states of the system is needed to construct the right-hand side of the equation, and efficient iterative algorithm can be used for the solution of the linear system. Doing so, the computational cost of the determination of the density response to a single perturbation is of the same order as that needed for the calculation of the unperturbed ground-state density. The left-hand side of Equation 2.15 is singular because the linear operator appearing therein has a null eigenvalue. However, we saw above that the response of the system to an external perturbation only depends on the component of the perturbation which couples the occupied-state manifold with the empty-state one. The projection onto the empty-state manifold of the first-order correction to occupied orbitals can be obtained from equation 2.15 by replacing its right-hand side with $-P_c\Delta|\Psi_n\rangle$, where P_c is the projector onto the empty-state manifold, and by adding to the linear operator on its left-hand side, $H_{SCF}-\epsilon_n$, a multiple of the projector onto the occupied state manifold, P_v, so as to make it non-singular

$$(H_{SCF} + \alpha P_v - \epsilon_n)|\Delta\Psi_n\rangle = -P_c\Delta V_{SCF}|\Psi_n\rangle \tag{2.20}$$

Virtually, if the linear system is solved by the conjugate-gradient or any other iterative method and the trial solution is chosen orthogonal to the occupied-state manifold, orthogonality is maintained during iteration without having to care about the extra P_v term on the left-hand side of equation 2.20.

In a very nutshell, the phonon calculation involves solving the secular equation 2.6 wherein the matrix of interatomic force constants is determined by the ground state charge density and its linear response to a perturbation.

while the ground state charge density is obtained using the scf procedure which fondamentally lies in solving iteratively the Kohn-Sham equations 1.9, the charge density linear response is calculated solving iteratively equations 2.17, 2.19 and 2.20. Hence, in the next section we will solve equations 2.6, 2.17, 2.19 and 2.20 for monochromatic perturbations in the case of crystalline solids.

2.2 Phonons and the Density Functional Perturbation Theory in a Computer

2.2.1 Phonons

In equation 2.6, the nucleus positions in the interatomic force constant are labelled by an index, n_i, which indicates the unit cell to which a given atom belongs, l, and the position of the atom within that unit cell, s: $n_i \equiv l, s$. The position of the n_i-th atom is thus:

$$\mathbf{R}_{n_i} \equiv \mathbf{R}_l + \mathbf{R}_s^{eq} + \mathbf{u}_s(l), \tag{2.21}$$

where $\mathbf{R}_l$ is the position of the l-th unit cell in the Bravais lattice, $\mathbf{R}_s^{eq}$ is the equilibrium position of the s-th atom in the unit cell, and $\mathbf{u}_s(l)$ indicates the deviation from equilibrium of the nuclear position. Because of translational invariance, the matrix of inter-atomic force constants in 2.7, changes with l and m only through the difference $\mathbf{R}_l - \mathbf{R}_m$:

$$\mathbf{C}_{st}^{\alpha\beta}(l,m) \equiv \frac{\partial^2 E}{\partial u_s^\alpha(l)\partial u_t^\beta(m)} = \mathbf{C}_{st}^{\alpha\beta}(\mathbf{R}_l - \mathbf{R}_m), \tag{2.22}$$

where the greek super-scripts indicate Cartesian components. The Fourier transform of $\mathbf{C}_{st}^{\alpha\beta}(\mathbf{R})$ with respect to $\mathbf{R}$, $\tilde{\mathbf{C}}_{st}^{\alpha\beta}(\mathbf{q})$, can be seen as the second derivative of the total energy with respect to the amplitude of a lattice distortion of definite wave-vector:

$$\tilde{\mathbf{C}}_{st}^{\alpha\beta}(\mathbf{q}) \equiv \sum_{\mathbf{R}} e^{-i\mathbf{q}\mathbf{R}}\mathbf{C}_{st}^{\alpha\beta}(\mathbf{R}) = \frac{1}{N_c}\frac{\partial^2 E}{\partial u_s^{*\alpha}(\mathbf{q})\partial u_t^\beta(\mathbf{q})} \tag{2.23}$$

where N_c is the number of unit cells in the crystal, and the vector $\mathbf{u}_s(\mathbf{q})$ is defined by the distortion pattern:

$$\mathbf{R}_{n_i}[\mathbf{u}_s(\mathbf{q})] = \mathbf{R}_l + \mathbf{R}_s^{eq} + \mathbf{u}_s(\mathbf{q})e^{-i\mathbf{q}\mathbf{R}_l}. \tag{2.24}$$

Phonon frequencies, $\omega(\mathbf{q})$, are solutions of the secular equation:

$$\det\left|\frac{1}{\sqrt{M_s M_t}}\tilde{\mathbf{C}}_{st}^{\alpha\beta}(\mathbf{q}) - \omega^2(\mathbf{q})\right| = 0 \tag{2.25}$$

Translational invariance can be alternatively stated in this context by saying that a lattice distortion of wavevector $\mathbf{q}$ does not induce a force response in the crystal at wave-vector $\mathbf{q}' \neq \mathbf{q}$. Because of this property, inter-atomic force constants are most easily calculated in reciprocal space and, when they are needed in direct space, they can be readily obtained by Fourier transform. The reciprocal-space expression for the matrix of inter-atomic force constants, in 2.7, is the sum of an electronic and of an nucleus contribution:

$$\tilde{\mathbf{C}}_{st}^{\alpha\beta}(\mathbf{q}) = {}^{el}\tilde{\mathbf{C}}_{st}^{\alpha\beta}(\mathbf{q}) + {}^{nu}\tilde{\mathbf{C}}_{st}^{\alpha\beta}(\mathbf{q}), \tag{2.26}$$

where

$${}^{el}\tilde{\mathbf{C}}_{st}^{\alpha\beta}(\mathbf{q}) = \frac{1}{N_c}\left[\int \frac{\partial^2 V_n}{\partial u_s^{*\alpha}(\mathbf{q})\partial u_t^{\beta}(\mathbf{q})} n(\mathbf{r})d\mathbf{r} + \int \frac{\partial n(\mathbf{r})}{\partial u_s^{\alpha}(\mathbf{q})}\frac{\partial V_n}{\partial u_t^{\beta}(\mathbf{q})} n(\mathbf{r})d\mathbf{r}\right], \tag{2.27}$$

and

$$V_n(\mathbf{q}) = \sum_{ls} v_s(\mathbf{r} - \mathbf{R}_l - \mathbf{R}_s^{eq} - \mathbf{u}_s(l)), \tag{2.28}$$

v_s being the pseudo-nucleus potential for the s-th atomic species. All the derivatives must be calculated for $u_s(\mathbf{q}) = 0$. The pseudo-nucleus contribution comes from the ion-ion interaction energy (the last term of 2.7) and does not depend on the electronic structure. Using 2.24 and 2.28, the derivatives of the potential appearing in 2.27 read:

$$\frac{\partial V_n}{\partial u_s^{\alpha}(\mathbf{q})} = -\sum_l \frac{\partial v_s(\mathbf{r} - \mathbf{R}_l - \mathbf{R}_s^{eq})}{\partial \mathbf{r}} e^{-i\mathbf{q}\mathbf{R}_l}, \tag{2.29}$$

while the corresponding derivative of the electron charge density distribution will be addressed in the next section.

2.2.2 Density Functional Perturbation Theory

One of the main points of DFPT is that within it, the responses to perturbations of different wave-lengths are decoupled. This feature allows one to calculate phonon frequencies at arbitrary wave-vectors $\mathbf{q}$ avoiding the use of supercells and with a workload which is essentially independent of the phonon wave-length. To see this in some detail, we first rewrite 2.20 by explicitly indicating the wave-vector $\mathbf{k}$ and band index v of the unperturbed wave-function, $\Psi_v^{\mathbf{k}}$, and by projecting both sides of the equation over the manifold of states of wave-vector $\mathbf{k}+\mathbf{q}$. Translational invariance requires that the projector onto the $\mathbf{k}+\mathbf{q}$ manifold, $P^{\mathbf{k}+\mathbf{q}}$, commutes with H_{SCF} and with the projectors onto the occupied- and empty-state manifolds, P_v and P_c. By indicating with $P^{\mathbf{k}+\mathbf{q}}P_v = P_v^{\mathbf{k}+\mathbf{q}}$ and $P^{\mathbf{k}+\mathbf{q}}P_c = P_c^{\mathbf{k}+\mathbf{q}}$ the projectors onto the occupied and empty states of wave-vector $\mathbf{k}+\mathbf{q}$, 2.20 can be rewritten as:

$$(H_{SCF} + \alpha P_v^{\mathbf{k}+\mathbf{q}} - \epsilon_v^{\mathbf{k}})|\Delta\Psi_v^{\mathbf{k}+\mathbf{q}}\rangle = -P_c^{\mathbf{k}+\mathbf{q}}\Delta V_{SCF}|\Psi_v^{\mathbf{k}}\rangle, \tag{2.30}$$

where $|\Delta\Psi_v^{\mathbf{k}+\mathbf{q}}\rangle = P^{\mathbf{k}+\mathbf{q}}|\Psi_v^{\mathbf{k}}\rangle$. Decomposing the perturbing potential, ΔV_{SCF}, into Fourier components,

$$\Delta V_{SCF}(\mathbf{r}) = \sum_{\mathbf{q}} \Delta v_{SCF}^{\mathbf{q}} e^{i\mathbf{q}\mathbf{r}} \tag{2.31}$$

where $\Delta v_{SCF}^{\mathbf{q}}$ is a lattice-periodic function, 2.30 becomes

$$\begin{aligned}\left(H_{SCF}^{\mathbf{k}+\mathbf{q}} + \alpha\sum_{v'}|u_{v'}^{\mathbf{k}+\mathbf{q}}\rangle\langle u_{v'}^{\mathbf{k}+\mathbf{q}}| - \epsilon_v^{\mathbf{k}}\right)|\Delta u_v^{\mathbf{k}+\mathbf{q}}\rangle \\ = -\left[1 - \sum_{v'}|u_{v'}^{\mathbf{k}+\mathbf{q}}\rangle\langle u_{v'}^{\mathbf{k}+\mathbf{q}}|\right]\Delta v_{SCF}^{\mathbf{q}}|u_v^{\mathbf{k}}\rangle\end{aligned} \tag{2.32}$$

where v' runs over the occupied states at $\mathbf{k}+\mathbf{q}$, $u_v^{\mathbf{k}}$ and $\Delta u_v^{\mathbf{k}+\mathbf{q}}$ are the periodic parts of the unperturbed wave-function and of the $\mathbf{k}+\mathbf{q}$ Fourier component of its first-order correction, respectively, and the coordinate representation kernel of the operator $H_{SCF}^{\mathbf{k}+\mathbf{q}}$, $h_{SCF}^{\mathbf{k}+\mathbf{q}}(\mathbf{r},\mathbf{r}') = \langle\mathbf{r}|H_{SCF}^{\mathbf{k}+\mathbf{q}}|\mathbf{r}'\rangle$ is defined in terms of the kernel of the SCF Hamiltonian, $h_{SCF}^0(\mathbf{r},\mathbf{r}') = \langle\mathbf{r}|H_{SCF}^{\mathbf{k}+\mathbf{q}}|\mathbf{r}'\rangle$, by the relation

$$h_{SCF}^{\mathbf{k}+\mathbf{q}}(\mathbf{r},\mathbf{r}') = e^{i(\mathbf{k}+\mathbf{q})\mathbf{r}}h_{SCF}^0(\mathbf{r},\mathbf{r}')e^{i(\mathbf{k}+\mathbf{q})\mathbf{r}'}. \tag{2.33}$$

2.32 shows that the time-consuming step of the self-consistent process, equation 2.20, can be carried on working on lattice-periodic functions only, and the corresponding numerical workload is therefore independent of the wavelength of the perturbation.

Let us now see how the other two steps of the selfconsistent process, 2.13 and 2.17, can be carried on in a similar way by treating each Fourier component of the perturbing potential and of the charge-density response independently. The Fourier components of any real function (such as Δn and Δv) with wavevectors $\mathbf{q}$ and $-\mathbf{q}$ are complex conjugate of each other: $\Delta n^{-\mathbf{q}}(\mathbf{r}) = (\Delta n^{\mathbf{q}}(\mathbf{r}))^*$, and likewise for the potential. Because of time-reversal symmetry, a similar results applies to wave-functions: $\Delta u_v^{\mathbf{k}+\mathbf{q}}(\mathbf{r}) = (\Delta u_v^{-\mathbf{k}-\mathbf{q}}(\mathbf{r}))^*$. Taking into account these relations, the Fourier component of the charge-density response at wave-vector $\mathbf{q}$ are obtained from Equation 2.13

$$\Delta n_v^{\mathbf{q}}(\mathbf{r}) = 4 \sum_{\mathbf{k}v} u_v^{\mathbf{k}*}(\mathbf{r}) \Delta u_v^{\mathbf{k}+\mathbf{q}}. \tag{2.34}$$

equation 2.17 displays a linear relation between the self-consistent variation of the potential and the variation of the electron charge-density distribution. The Fourier component of the self-consistent potential response reads:

$$\Delta v_{SCF}^{\mathbf{q}}(\mathbf{r}) = \Delta v^{\mathbf{q}}(\mathbf{r}) + e^2 \int \frac{\Delta n_v^{\mathbf{q}}(\mathbf{r}')}{|\mathbf{r} - \mathbf{r}'|} e^{i\mathbf{q}(\mathbf{r}-\mathbf{r}')} d\mathbf{r}' + \left. \frac{dv_{x-c}(n)}{dn} \right|_{n=n(\mathbf{r})} \Delta n_v^{\mathbf{q}}(\mathbf{r}) \tag{2.35}$$

The sampling of the Brillouin Zone needed for the evaluation of 2.34 is similar to that needed for the calculation of the unperturbed electron charge density.

In conclusion, equations 2.32, 2.34, and 2.35 form a set of self-consistent relations for the charge-density and wavefunction linear response to a perturbation of a wavevector, $\mathbf{q}$, which can be solved in terms of lattice-periodic functions only, and which is decoupled from all the other sets of similar equations holding for other Fourier components of same perturbation. The most computationally demanding process for the whole phonon calcultation is the evaluation of the interatomic force constants. As a matter of fact, the eval-

uation of the dynamical matrices on a regular grid of wave-vectors in the Brillouin Zone, whose spacing must be chosen of the order of the inverse of the range of the matrix (labelled R_{IFC}): $\Delta\mathbf{q} \sim 2\pi/R_{IFC}$. The number of $\mathbf{q}$-points in such a grid is of the order of R_{IFC}^3. As the computational cost for the calculation of each column of the dynamical matrix is of the order of N_{at}^3 (and the number of such columns is $3N_{at}$) the total cost for the dynamical matrix calculation (and, hence, of complete phonon dispersions) using DFPT is of the order of $R_{IFC}^3 \times 3N_{at}^4$. In the next section we present and discuss the results.

2.3 Results and Discussion

The calculation of the ground state charge density was performed through the self-consistent procedure with the same parameters as the band structure calculation and a $\mathbf{k}$-point grid $4 \times 4 \times 1$ dense. The phonon calculation is performed with a $\mathbf{q}$-vector grid of $4 \times 4 \times 4$ either for the hexagonal or the FCC phase. The phonon calculation took around 2 weeks for the hexagonal phase and a month for the FCC phase on a 8-processor Linux cluster. The convergence threshold for the phonon calculation has been set to 10^{-12} for the hexagonal phase and 10^{-14} for the FCC phase. Figure 2.1 shows the

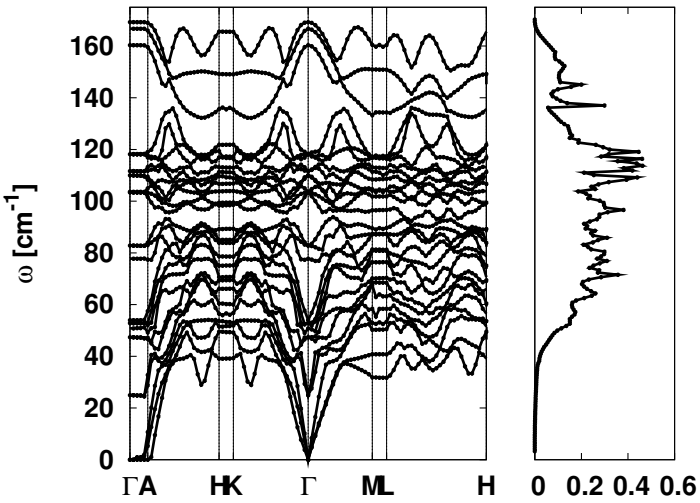

Figure 2.1: Phonon dispersion (left) and spectrum (right) for the hexagonal phase.

calculated phonon spectrum and the corresponding phonon density of states of the hexagonal phase. The phonon dispersion shows a set of 27 branches that stretches from 0 to $\sim$ 165 cm^{-1}. On the contrary, the FCC phonon

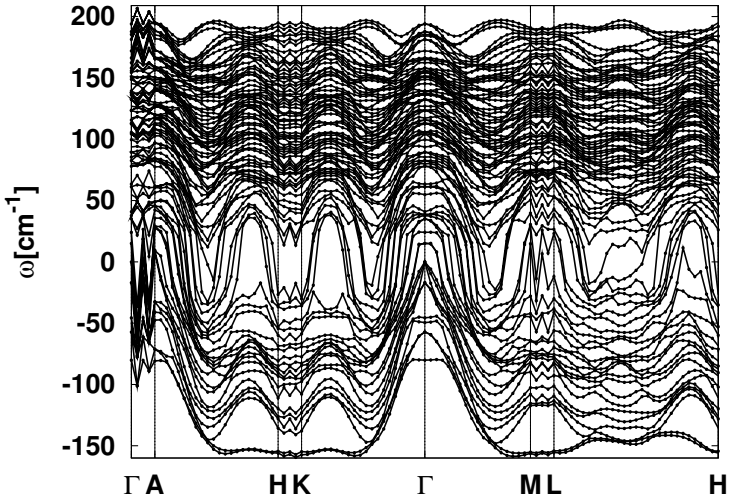

Figure 2.2: Phonon dispersion for the FCC phase.

dispersion (see figure 2.2) and density of phonon states (figure 2.3) show a set of 81 branches spanning from ~ -160 to $\sim$ 210 cm^{-1}. The negative frequencies for the FCC phase signal the instabily of the structure. Non-surprisingly, the FCC structure is referred to as meta-stable to make it easier for the transition to the amorphous phase to take place.

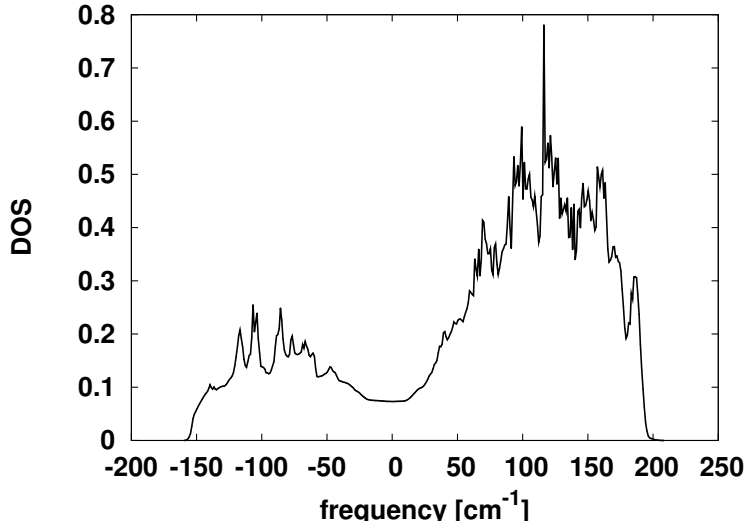

Figure 2.3: Phonon spectrum for the FCC phase.

Chapter 3

Optical Properties

Largely, a material optical response is paramount to its investigation because it provides detailed information about the band gap and the electronic state occupancy. This is specially foundational for chalcogenides because they were primarily used for optical-storage devices. In this instance, the meaningful difference in reflectivity depending on the phase the material is in, tells apart two binary digits. In this section we figure out how the photon energy ω changes the optical constants such as the dielectric function ϵ (both real and imaginary parts), the refractive index n, the extinction coefficient k, the absorption coefficient α, the optical transmission T and reflection R. We will also figure out the thickness dependence of $T(\omega)$ and $R(\omega)$. What follows is thus organized into a methodology and a result sections. In the methodology section, a three fold picture of optical constants is given based on light as a ray, a wave or a beam of corpuscules. Although the ray-like and wave-like pictures are basic and elementary, a brief summary is helpful for a better understanding of corpuscule-like or microscopic calcultations. Then the result section discloses and comments the comparison between calculated and measured optical properties.

3.1 Methodology and Computational Details

3.1.1 Methodology

Optical Constants: the ray-like perspective

Let us begin by stating that how much light velocity is curbed in a medium defines the refractive index of that medium

$$n_{m_i} = c/v_{m_i}, \tag{3.1}$$

m_i being the i-th medium. When a light ray of intensity $\mathbf{I}_0$ at an incidence angle $\hat{i}$ shines on the interface between two mediums m_1 and m_2, where m_2 is a material z thick, part of it is reflected at an angle $\hat{r}$, the remaining part goes through the material bending at an angle of $\hat{t}$ and with an intensity of $\mathbf{I}$. *Snell-Descartes*'s law of refraction

$$n_{m_1} \sin(\hat{i}) = n_{m_2} \sin(\hat{t}), \tag{3.2}$$

links the two medium refractive indexes, *Beer-Lambert*'s law

$$\mathbf{I} = \mathbf{I}_0 e^{-\alpha z}, \tag{3.3}$$

defines the intensity attenuation as *absorption coefficient*, α. *Fresnel*'s equations

$$\begin{aligned} R &= \frac{\sin(\hat{t} - \hat{i})}{\sin(\hat{t} + \hat{i})} \\ T + R &= 1, \end{aligned} \tag{3.4}$$

relate the transmitted T and reflected light R together and to the angles $\hat{i}$, $\hat{r}$ and $\hat{t}$.

Optical constants: the wave-like perspective

Let us think of a light ray going through a material as an electromagnetic wave propagating in the z direction of a lossy medium. The electric part of the wave equation thus comes down to

$$\frac{\partial^2 E_x}{\partial z^2} = i\omega\mu_0(\sigma + i\epsilon\omega)E_x = \Gamma^2 E_x \tag{3.5}$$

where the conductivity σ and the dielectric constant ϵ are defined within the Maxwell equations.

$$\Gamma = \sqrt{i\omega\mu_0(\sigma + i\epsilon\omega)} = (\alpha/2) + i\beta \tag{3.6}$$

is the *complex propagation constant*. The ratio

$$\frac{\Gamma}{\Gamma_0} = -\tilde{n}^2 \tag{3.7}$$

where Γ_0 is the propagation constant in a free space ($\sigma = 0$, $\epsilon = \epsilon_0$) defines the *complex refractive index* $\tilde{n} = n + ik$ with a real part (refractive index) and an imaginary called *extinction coefficient*. Moreover, 3.1 with $c = 1/\sqrt{\mu_0\epsilon_0}$ and $v_{m_i} = 1/\sqrt{\mu_0\epsilon}$ leads to $\tilde{n}^2 = \epsilon/\epsilon_0 = \epsilon_r + i\epsilon_i$. The real and imaginary parts of the dielectric function are thus related to the complex refractive index through the following relations

$$\begin{aligned} n^2 - k^2 &= \epsilon_r \\ 2nk &= -\epsilon_i. \end{aligned} \tag{3.8}$$

The absorption coefficient α appearing in equation 3.6 is therefore determined as

$$\alpha = \frac{4\pi k}{\lambda}. \tag{3.9}$$

Optical constants: the corpuscule-like perspective

From equations 3.8, 3.9 and 3.4, it stands out that the knowledge of the dielectric function ϵ is sufficient to derive all other optical constants. The whole dielectric tensor is calculted and then the diagonal terms are extracted out of it.

Seeing light as a set quasi-particles, photons, leads to interpret its interaction with matter as absorption or emision of such photons by electrons. The microscopic effect of it is a certain number of electron transitions within and between the valence and the conduction bands. The imaginary part of the dielectric tensor $\epsilon_{i_{\alpha,\beta}}(\omega)$ can be thus viewed as a response function that comes

from a perturbation theory with adiabatic turning on:

$$\epsilon_{\alpha,\beta}(\omega) = 1 + \frac{4\pi e^2}{\Omega N_{\mathbf{k}} m^2} \sum_{n,n'} \sum_{\mathbf{k}} \frac{\hat{\mathbf{M}}_{\alpha,\beta}}{(E_{\mathbf{k},n'} - E_{\mathbf{k},n})^2} \cdots$$

$$\cdots \Bigg\{ \frac{f(E_{\mathbf{k},n})}{E_{\mathbf{k},n'} - E_{\mathbf{k},n} + \hbar\omega + i\hbar\Gamma} + \cdots$$

$$\cdots \frac{f(E_{\mathbf{k},n})}{E_{\mathbf{k},n'} - E_{\mathbf{k},n} - \hbar\omega - i\hbar\Gamma} \Bigg\} \tag{3.10}$$

where Γ is the adiabatic parameter which, for the total energy conservation must tend to zero. This is the way in which the Dirac Delta function appears and this means that every excited state has an infinite lifetime, i.e., is stationary.

$$\epsilon_{i_{\alpha,\beta}}(\omega) = \frac{4\pi e^2}{\Omega N_{\mathbf{k}} m^2} \sum_{n,n'} \sum_{\mathbf{k}} \frac{\hat{\mathbf{M}}_{\alpha,\beta} f(E_{\mathbf{k},n})}{(E_{\mathbf{k},n'} - E_{\mathbf{k},n})^2} \cdots$$

$$\cdots \Big[\delta(E_{\mathbf{k},n'} - E_{\mathbf{k},n} + \hbar\omega) + \delta(E_{\mathbf{k},n'} - E_{\mathbf{k},n} - \hbar\omega) \Big] \tag{3.11}$$

This situation is unphysical because the interaction with electromagnetic field (even in the absence of photons, i.e., spontaneous emission) gives an intrinsic broadening to all exited states, the lifetime is finite and Γ must be larger than zero. In the limit of small but non vanishing Γ the dielectric tensor turns into the Drude-Lorentz one:

$$\epsilon_{i_{\alpha,\beta}}(\omega) = \frac{4\pi e^2}{\Omega N_{\mathbf{k}} m^2} \sum_{n,\mathbf{k}} \frac{df(E_{\mathbf{k},n})}{dE_{\mathbf{k},n}} \frac{\eta\omega \hat{\mathbf{M}}_{\alpha,\beta}}{\omega^4 + \eta^2\omega^2} + \cdots$$

$$\cdots + \frac{8\pi e^2}{\Omega N_{\mathbf{k}} m^2} \sum_{n \neq n'} \sum_{\mathbf{k}} \frac{\hat{\mathbf{M}}_{\alpha,\beta}}{E_{\mathbf{k},n'} - E_{\mathbf{k},n}} \cdots$$

$$\cdots \frac{\Gamma\omega f(E_{\mathbf{k},n})}{\left[(\omega_{\mathbf{k},n'} - \omega_{\mathbf{k},n})^2 - \omega^2\right]^2 + \Gamma^2\omega^2} \tag{3.12}$$

while the real part comes from the Kramers-Kronig transformation:

$$\epsilon_{r_{\alpha,\beta}}(\omega) = 1 + \frac{2}{\pi} \int_0^\infty \frac{\omega' \epsilon_{i_{\alpha,\beta}}(\omega')}{\omega'^2 - \omega^2} d\omega' \tag{3.13}$$

$$\epsilon_{r_{\alpha,\beta}}(\omega) = 1 - \frac{4\pi e^2}{\Omega N_{\mathbf{k}} m^2} \sum_{n,\mathbf{k}} \frac{df(E_{\mathbf{k},n})}{dE_{\mathbf{k},n}} \frac{\omega^2 \hat{\mathbf{M}}_{\alpha,\beta}}{\omega^4 + \eta^2\omega^2} + ...$$

$$... + \frac{8\pi e^2}{\Omega N_{\mathbf{k}} m^2} \sum_{n \neq n'} \sum_{\mathbf{k}} \frac{\hat{\mathbf{M}}_{\alpha,\beta}}{E_{\mathbf{k},n'} - E_{\mathbf{k},n}} ...$$

$$... \frac{\left[(\omega_{\mathbf{k},n'} - \omega_{\mathbf{k},n})^2 - \omega^2\right] f(E_{\mathbf{k},n})}{\left[(\omega_{\mathbf{k},n'} - \omega_{\mathbf{k},n})^2 - \omega^2\right]^2 + \Gamma^2\omega^2} \tag{3.14}$$

Finally the complex dielectric function is:

$$\epsilon_{\alpha,\beta}(\omega) = 1 - \frac{4\pi e^2}{\Omega N_{\mathbf{k}} m^2} \sum_{n,\mathbf{k}} \frac{df(E_{\mathbf{k},n})}{dE_{\mathbf{k},n}} \frac{\hat{\mathbf{M}}_{\alpha,\beta}}{\omega^2 + i\eta\omega} + ...$$

$$... + \frac{8\pi e^2}{\Omega N_{\mathbf{k}} m^2} \sum_{n' \neq n} \sum_{\mathbf{k}} \frac{\hat{\mathbf{M}}_{\alpha,\beta}}{(E_{\mathbf{k},n'} - E_{\mathbf{k},n})} ...$$

$$... \frac{f(E_{\mathbf{k},n})}{(\omega_{\mathbf{k},n'} - \omega_{\mathbf{k},n})^2 + \omega^2 + i\Gamma\omega}$$

Γ and η are respectively *intersmear* and *intrasmear* parameters. The square matrix elements are defined as follow:

$$\hat{\mathbf{M}}_{\alpha,\beta} = \langle u_{\mathbf{k},n'} | \hat{\mathbf{p}}_\alpha | u_{\mathbf{k},n} \rangle \langle u_{\mathbf{k},n} | \hat{\mathbf{p}}^\dagger_\beta | u_{\mathbf{k},n'} \rangle \tag{3.15}$$

$$\propto u^\star_{\mathbf{k},n'}(\mathbf{r}) \frac{d}{dx_\alpha} u_{\mathbf{k},n}(\mathbf{r}) u^\star_{\mathbf{k},n}(\mathbf{r}) \frac{d}{dx_\beta} u_{\mathbf{k},n'}(\mathbf{r}) \tag{3.16}$$

the double index reveals the tensorial nature of $\epsilon_i(\omega)$, while $|u_{\mathbf{k},n}\rangle$ is a factor of the single-particle Bloch function obtained with a self-consistent calculation. In all the cases illustrated above the non-local contribution due to the pseudopotential is neglected, actually the correction to the matrix element that takes into account the non-local part of the Hamiltonian is not implemented. From the previous definition of the imaginary part of the dielectric function it is easy to see that even the local-field contributions are not implemented.

The self consistent calculation works on a plane wave set so the Bloch functions of the matrix element (3.15) are decomposed as follow:

$$|\psi_{\mathbf{k},n}\rangle = e^{i\mathbf{G}\cdot\mathbf{r}} u_{\mathbf{k},n} = \frac{1}{\sqrt{V}} \sum_{\mathbf{G}} a_{n,\mathbf{k},\mathbf{G}} e^{i(\mathbf{k}+\mathbf{G})\cdot\mathbf{r}} \tag{3.17}$$

and consequently:

$$\hat{\mathbf{M}}_{\alpha,\beta} = \left(\sum_{\mathbf{G}} a^{\star}_{n,\mathbf{k},\mathbf{G}} a_{n',\mathbf{k},\mathbf{G}} G_{\alpha} \right) \left(\sum_{\mathbf{G}} a^{\star}_{n,\mathbf{k},\mathbf{G}} a_{n',\mathbf{k},\mathbf{G}} G_{\beta} \right) \tag{3.18}$$

Defined in this way the matrix element accounts only for interband transitions, i.e., vertical transitions in which the electron momentum $\mathbf{k}$ is conserved (optical approximation). In standard optics the intraband transitions give a negligible contribution due to the very low momentum transferred by the incoming/outcoming photon.
Operating a London transformation upon $\epsilon_{i_{\alpha,\beta}}(\omega)$, it's possible to obtain the whole dielectric tensor calculated on the imaginary frequency axe $\epsilon_{\alpha,\beta}(i\omega)$.

$$\epsilon_{\alpha,\beta}(i\omega) = 1 + \frac{2}{\pi} \int_0^{\infty} \frac{\omega' \epsilon_{i_{\alpha,\beta}}(\omega')}{\omega'^2 + \omega^2} d\omega' \tag{3.19}$$

The dielectric function being calculated, the refractive index, the extentive and absorption coefficient are obtained through 3.8 and 3.9. As it relates to the optical transmission $T(\omega)$ and reflection ω, it should be pointed out that equations 3.4 hold at the interface with the theoretical infinite sample. In most practical cases instead, $Ge_2Sb_2Te_5$ samples are available as thin films on substrates. What's more, unlike other optical constants, $T(\omega)$ and $R(\omega)$ vary significantly with the film thickness. For this matter, $[T(\omega), R(\omega)]$ thickness dependence is introduced through exact optical equations for a normally incident light on a thin layer on top of a thick substrate [26]. A transparent substrate with $n = 1.5$ and $k = 0$ is assumed for this post-processing because a glass slide has similar properties especially between $\omega \sim 0.4$ and $\omega \sim 4$ eV.

3.1.2 Computational Details

As equation 3.1.1 needs both ground and excited states to be computed, a self-consistent calculation is performed using grid of $12 \times 12 \times 4$ and $12 \times 12 \times 2$ for the hexagonal and FCC phases respectively using the same parameters and the band diagram and density of electronic state calculations. A uniform grid of $20 \times 20 \times 20$ is used in the non-self consistent calculation for the

excited states. The non-self-consistent calculation took roughly 2 days for the hexagonal phase and 6 days for the FCC phase. Such a very dense grid is used to increase the accuracy on the excited charge density mainly responsible for the excited states since the self-consistency doesn't apply here. The parameters Γ (*intersmear*) and η (*intrasmear*) are set to 1.0 and 1.0 for the hexagonal phase and 0.8 and 0.3 for the face-centered cubic state to best fit experimental data.

3.2 Results and Discussion

The calculated real and imaginary parts of the hexagonal dielectric function are presented in figure 3.1. The comparison with the measured ones is appreciable even though there is a shift in the energy axis that will be explained further on. Figure 3.2 shows pretty much the same agreement and the same shift in the energy axis between calculated and experimental [2, 1] ϵ_r and ϵ_i for the face-centered cubic phase. The magnitude difference in figures 3.1, 3.2 for small energy values are mainly due to the fact that for small energy differences in the denominator of expressions 3.1.1 and 3.1.1, $\epsilon_i(\omega)$ and $\epsilon_r(\omega)$ tend to diverge. The magnitude difference around the peak result from transistions between the top of the valence band and the bottom of the conduction band is not accurately described because of the inaccuracy of the band gap for the reasons laid out in the sub-section *"Local Density Approximation and the Band Gap"*. As the calculated band gap is smaller than the experimental one, it stands to reason that by virtue of equations 3.1.1 and 3.1.1, the peak of the calculated curve is higher than the experimental one.

The calculated and experimental [2] refractive index and extinctive coefficient are also compared for the hexagonal (figure 3.3) and FCC (figure 3.4) structures. As $n(\omega)$ and $k(\omega)$ vary directly with $\epsilon_i(\omega)$ and $\epsilon_r(\omega)$, the same reasons behind the experimental and calculated FCC dielectric function discrepancies apply here even though it should be pointed out a better matching for the FCC refractive index and extinctive coefficient. This can

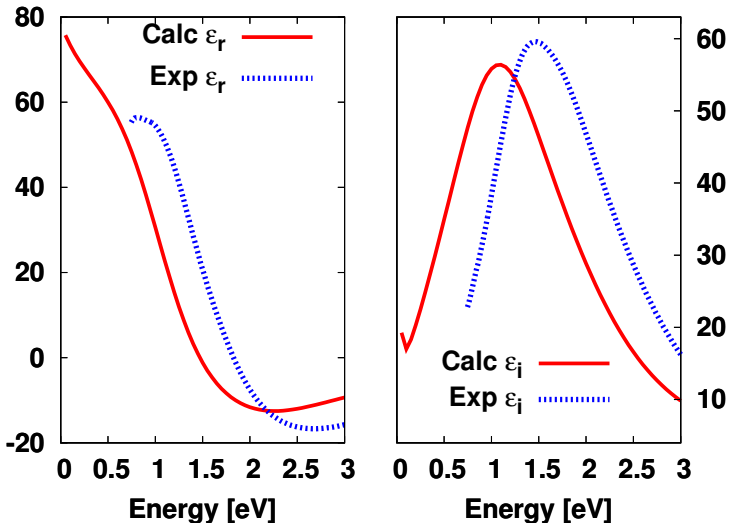

Figure 3.1: Calculated and experimental real (left) and imaginary (right) parts of the hexagonal dielectric function.

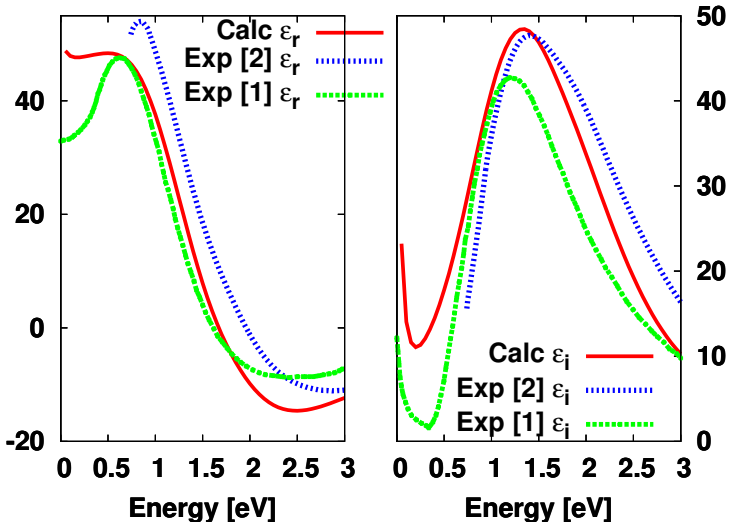

Figure 3.2: Calculated and experimental real (left) and imaginary (right) parts of the fcc dielectric function.

be ascribed to the fact that FCC band gap is closer to the experimental one. This is especially true for the peak differences. Figure 3.5 shows the calculated and experimental [2] absorption coefficient for the hexagonal and FCC phases. Here too, the FCC absorption coefficient better accords with the experimental one because its calculated band gap is closer to the measured one.

As to the optical transmission and reflection, figure 3.6 and 3.7 shows the

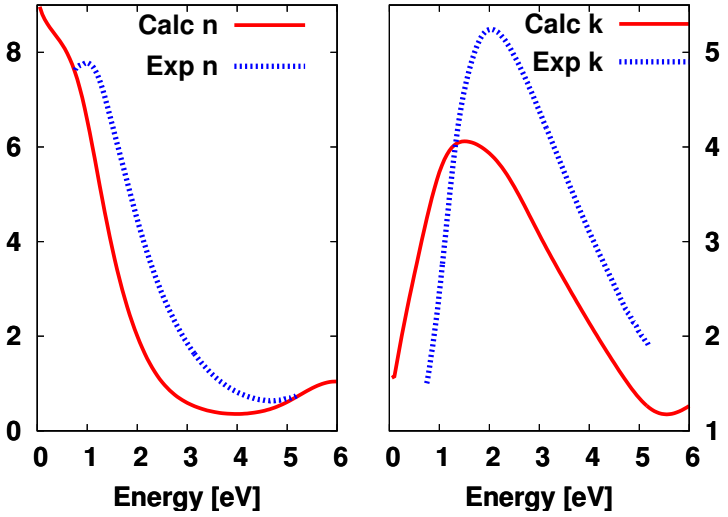

Figure 3.3: Calculated vs experimental refractive index (left) and extinctive coefficient (right) for the hexagonal phase.

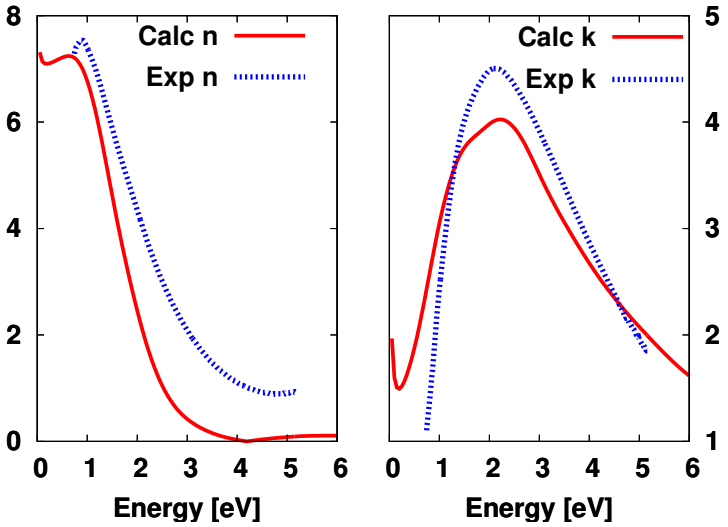

Figure 3.4: Calculated vs experimental refractive index (left) and extinctive coefficient (right) for the fcc phase.

simulated $T(\omega)$ and $R(\omega)$ for various thickness values of $Ge_2Sb_2Te_5$. Interference fringes are apparent in the spectra near or below the optical bandgap, since multiple reflections occur inside the film and interfere with each other. On top of that, in both figures $T(\omega)$ scales down with the thickness as intuitively expected. Conversely, $R(\omega)$ scales up with the thickness as expected by experiments. This calculated $[T(\omega), R(\omega)]$ thickness dependence reasonably line up with the experiments (see figures 3.8 for the hexagonal phase

and 3.9 for th FCC phase). Similar interference fringe patterns appear at lower photon energies in the calculated spectra than in the measured data, since the calculated bandgap values are lower than the measured ones.

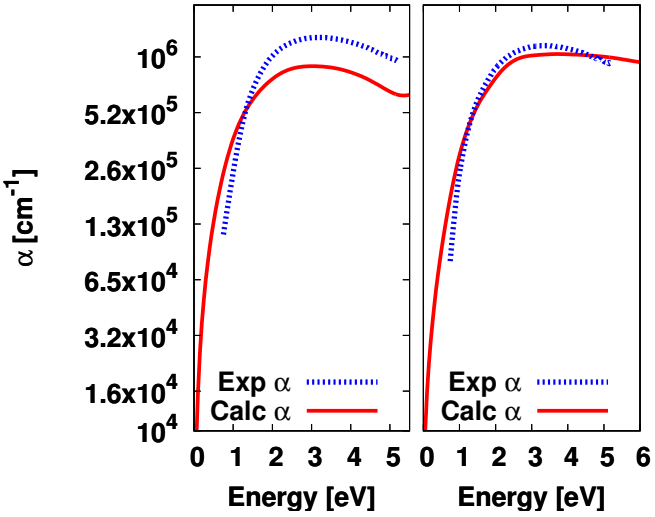

Figure 3.5: Calculated and experimental absorption coefficient for the hexagonal (left) and FCC (right) phases.

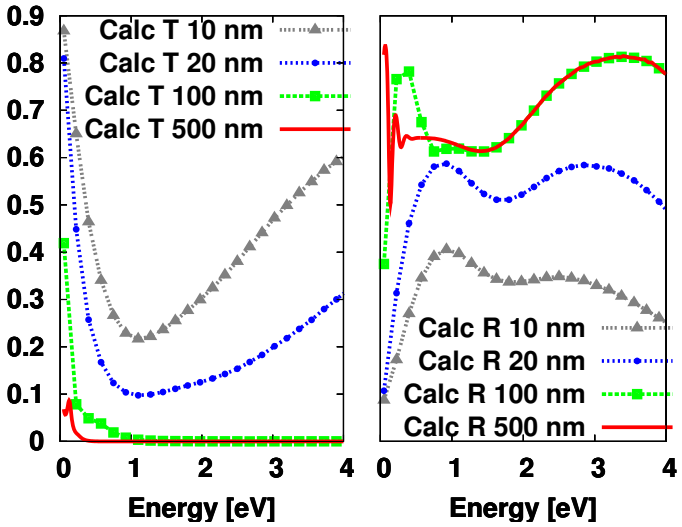

Figure 3.6: Calculated optical transmission (left) and reflection (right) reflection changing with the thickness for the hexagonal phase.

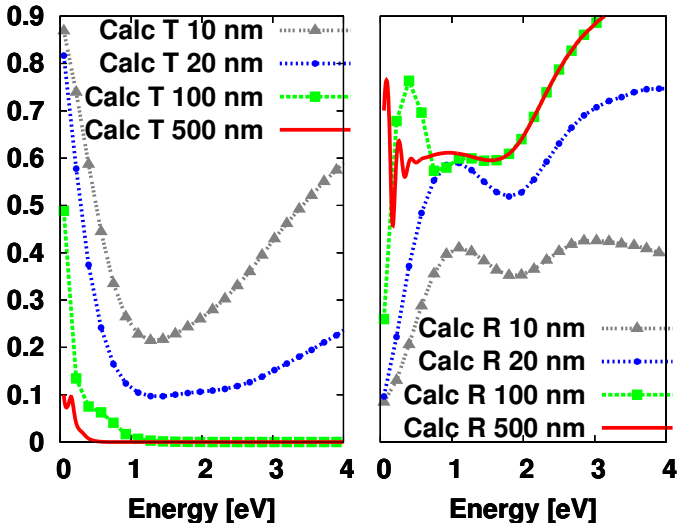

Figure 3.7: Calculated optical transmission (left) and reflection (right) reflection changing with the thickness for the fcc phase.

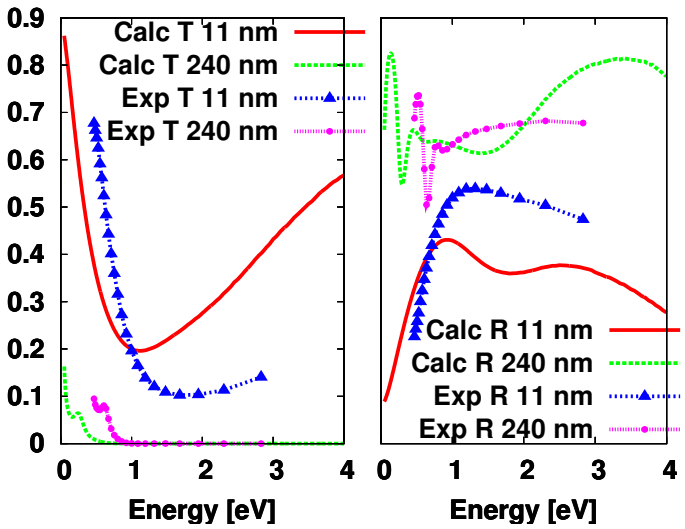

Figure 3.8: Calculated and experimental thickness dependence of T (left) and R for the hexagonal phase.

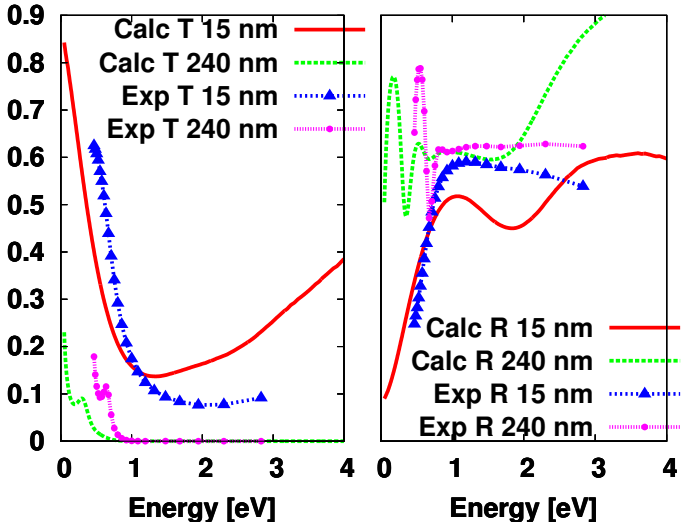

Figure 3.9: Calculated and experimental thickness dependence of T (left) and R for the fcc phase.

Conclusion

To sum it up, the electronic, vibrational and optical properties for the hexagonal and FCC phases of the $Ge_2Sb_2Te_5$ chalcogenide have been addressed. As it relates to the electronic properties, the electronic band diagram and density of states were calculated using the density functional theory combined with plane waves, norm-conserving pseudopotentials and the local density approximation implemented in the code *Quantum Espresso* [27]. Hexagonal band diagram and density of states agrees well with those calculated with *castep* [14]. As a matter of fact both exhibit a 0.0 eV band gap. FCC band diagram and density of states are shown with a band gap of about 0.10 eV and it should be pointed out that the FCC density of states remarkably lines up with the experimental one. The increase in the calculated band gap can be explained by the defect increase in the structure (no vacancy in the hexagonal primitive cell, 3 vacancies in the FCC primitive cell). The difference between the calculated band gap for both phases and the experimental one mainly originates from the local density approximation in the DFT calculations.
As far as the optical properties are concerned, the real part of the dielectric function was obtained implementing the Drude-Lorentz expression whereas the imaginary part was derived through the Kramers-Kronig relationship. Further, the refractive index, the extinctive and absorption coefficients are derived from the Maxwell model. The optical transmission and reflection are calculated. The calculated and measured thickness dependence of such quantities successfully compared. The discrepancies are mainly related to the inaccuracy in the calculated band gap that makes the transitions be-

tween valence and conduction states not exactly reproducible.

The density-functional perturbation theory allowed us to calculate the phonon dispersion and spectra for both phases. The results confirmed the chalcogenide tendency to have very low phonon frequency. The negative phonon frequencies obtained for the FCC phase is ascribed to the FCC instability mostly due to the high percentage of vacancy (20%). In fact, as opposed to the hexagonal stable phase, FCC's is referred to as metastable .

Appendix A

A.1 The Hohenberg and Kohn Theorems

A.1.1 Proof of Theorem I: density as a basic variable

Let us suppose two different external potentials $\hat{V}_n^{(1)}$ and $\hat{V}_n^{(2)}$ differing by more than a constant and both corresponding to the same ground state density $n_0(\mathbf{r})$. As a result, $\hat{V}_n^{(1)}$ and $\hat{V}_n^{(2)}$ lead to $\hat{H}^{(1)}$ and $\hat{H}^{(2)}$ which in turn yield two different wavefunctions, $\Psi^{(1)}$ and $\Psi^{(2)}$ respectively. As $\Psi^{(2)}$ is not the ground state of $\hat{H}^{(1)}$, it follows that

$$E^{(1)} = \langle \Psi^{(1)} | \hat{H}^{(1)} | \Psi^{(1)} \rangle < \langle \Psi^{(2)} | \hat{H}^{(1)} | \Psi^{(2)} \rangle. \tag{A.1}$$

where the strict inequality holds if the ground state is non-degenerate. The last term in A.1 can be written

$$\begin{aligned} \langle \Psi^{(2)} | \hat{H}^{(1)} | \Psi^{(2)} \rangle &= \langle \Psi^{(2)} | \hat{H}^{(2)} | \Psi^{(2)} \rangle + \langle \Psi^{(2)} | \hat{H}^{(1)} - \hat{H}^{(2)} | \Psi^{(2)} \rangle & \text{(A.2)} \\ &= E^{(2)} + \int d^3\mathbf{r} [\hat{V}_n^{(1)} - \hat{V}_n^{(2)}] n_0(\mathbf{r}) & \text{(A.3)} \end{aligned}$$

such that

$$E^{(1)} < E^{(2)} + \int d^3\mathbf{r} [\hat{V}_n^{(1)} - \hat{V}_n^{(2)}] n_0(\mathbf{r}) \tag{A.4}$$

Likewise for $E^{(2)}$, we find the same equation with superscripts (1) and (2) interchanged,

$$E^{(2)} < E^{(1)} + \int d^3\mathbf{r} [\hat{V}_n^{(2)} - \hat{V}_n^{(1)}] n_0(\mathbf{r}) \tag{A.5}$$

Combining A.4 and A.5, we cannot help but get to the contradictory inequality $E^{(1)} + E^{(2)} < E^{(1)} + E^{(2)}$ which establishes the desired results, that is, there cannot be two different external potentials differing by more than a constant for the same non-degenerate ground state charge density. Therefore, the density uniquely determines the external potential within a constant.
The corollary follows since the Hamiltonian is uniquely determined (except for a constant) by the ground state density. Then, in principle, the wavefunction of any state is determined by solving the Shrödinger equation with this Hamiltonian. Among all the solutions which are consistent with the given density, the unique ground state wavefunction is the one that has the lowest energy.

A.1.2 Proof of Theorem II

This theorem is a straighfoward consequence of the first on condition that one carefully defines the meaning of the functional of the density and restricts the space of densities. The original Proof of Hohenberg and Kohn is restricted to densities $n(\mathbf{r})$ that are ground state densities of the electron Hamiltonian with some external potential $\hat{V}_n$. Such densities are called "V-representable". This defines a space of possible densities within which we can construct *functionals* of the density. Since all properties such as kinetic energy and so forth are uniquely determined if $n(\mathbf{r})$ is specified, then each property can be viewed as a functional of $n(\mathbf{r})$, including the total energy functional

$$\begin{aligned} E[n] &= \langle\Psi|\hat{T}_e + \hat{V}_{ee} + \hat{V}_n|\Psi\rangle \\ &= \langle\Psi|\hat{T}_e + \hat{V}_{ee}|\Psi\rangle + \langle\Psi|\hat{V}_n|\Psi\rangle \\ &= F[n(\mathbf{r})] + \int n(\mathbf{r})\hat{V}_n d\mathbf{r} \end{aligned} \tag{A.6}$$

where $F[n(\mathbf{r})]$ must be universal by construction since the kinetic energy and interaction energy of particles are functionals of the density only.
Considering now a system with the ground state density $n^{(1)}(\mathbf{r})$ corresponding to an external potential $\hat{V}_n^{(1)}$, based on what just mentioned, the Hohenberg-Kohn functional is equal to the expectation value of the Hamiltonian in the

unique ground state, which has a wavefunction $\Psi^{(1)}$ such that

$$E^{(1)} = E[n^{(1)}] = \langle \Psi^{(1)} | \hat{H}^{(1)} | \Psi^{(1)} \rangle. \tag{A.7}$$

Similarly a different density $n^{(2)}(\mathbf{r})$ with $\Psi^{(2)}$ will lead to an energy

$$E^{(2)} = \langle \Psi^{(2)} | \hat{H}^{(1)} | \Psi^{(2)} \rangle > \langle \Psi^{(1)} | \hat{H}^{(1)} | \Psi^{(1)} \rangle = E^{(1)}. \tag{A.8}$$

Thus the energy given by A.6 in terms of the Hohenberg-Kohn functional evaluated for the correct ground state density $n_0(\mathbf{r})$ is indeed lower than the value of this expression for any other density $n(\mathbf{r})$.
It follows that if the functional $F[n(\mathbf{r})]$ was known, then by minimizing the total energy of the system, A.6, with respect to variations in the density function $n(\mathbf{r})$, one would find the exact ground state density and energy. This establishes Corollary **II**.

A.2 Kohn and Sham Equations

From Kohn and Sham's perspective, the interacting system can be replaced by a non-interactive one having the same ground state charge density $n_0(\mathbf{r})$. The charge density of such an auxiliary system

$$n(\mathbf{r}) = 2 \sum_{i}^{N_e} |\Psi_i(\mathbf{r})|^2 dr \tag{A.9}$$

rests on the non-interacting electron orbitals $\Psi_i(\mathbf{r})$ resulting from

$$[\hat{T}_e^{n-int} + \hat{V}_n] \Psi_i(\mathbf{r}) = \epsilon_i \Psi_i(\mathbf{r}) \tag{A.10}$$

and abiding by the orthonormality constraints

$$\int \Psi_i^*(\mathbf{r}) \Psi_j(\mathbf{r}) = \delta_{ij}. \tag{A.11}$$

The existence of a unique potential $\hat{V}_n$ having $n_0(\mathbf{r})$ as its ground state charge density is a consequence of the Hohenberg and Kohn theorem, which holds irrespective of the form of the electron-electron interaction $\hat{V}_{ee}$.

The purpose is to determine $\hat{V}_n$ for a given $n(\mathbf{r})$. This problem is solved by considering the variational property of the energy. For an arbitrary variation of the orbital $\Psi_i(\mathbf{r})$, under the orthonormality constraints of Eq. A.11, the variation of E must vanish. This means that the functional derivative with respect to the wavefunction $\Psi_i(\mathbf{r})$ of the constrained functional

$$E^{'} = E - \sum_{ij} \lambda_{ij} (\int \Psi_i^*(\mathbf{r}) \Psi_j(\mathbf{r}) - \delta_{ij}), \tag{A.12}$$

where λ_{ij} are Lagrange multipliers, must vanish:

$$\frac{\partial E}{\partial \Psi_i^*(\mathbf{r})} = \frac{\partial E^{'}}{\partial \Psi_i(\mathbf{r})} = 0. \tag{A.13}$$

Let us re-write the energy functional as follows:

$$E = T_{n-int}[n(\mathbf{r})] + E_H[n(\mathbf{r})] + E_{x-c}[n(\mathbf{r})] + \int n(\mathbf{r}) + \hat{V}_n d\mathbf{r}, \tag{A.14}$$

where the first term is the kinetic energy of non-interacting electrons

$$T_{n-int}[n(\mathbf{r})] = -\frac{\hbar^2}{2m} 2 \sum_i \int \Psi_i^*(\mathbf{r}) \nabla^2 \Psi_j(\mathbf{r}) d\mathbf{r}. \tag{A.15}$$

The second term (called the Hartree energy) contains the electrostatic interactions between clouds of charge

$$E_H[n(\mathbf{r})] = \frac{e^2}{2} \int \frac{n(\mathbf{r}) n^{'}(\mathbf{r}^{'})}{|\mathbf{r} - \mathbf{r}^{'}|} d\mathbf{r} d\mathbf{r}^{'}. \tag{A.16}$$

The third term, called the *exchange-correlation energy*, contains all the remaining terms. Knowing that

$$\frac{\partial n(\mathbf{r})}{\partial \Psi_i^*(\mathbf{r})} = \Psi_i(\mathbf{r}) \delta(\mathbf{r} - \mathbf{r}^{'}). \tag{A.17}$$

$$\frac{\partial T_{n-int}}{\partial \Psi_i^*(\mathbf{r})} = -\frac{\hbar^2}{2m} 2 \sum_i \nabla^2 \Psi_i(\mathbf{r}). \tag{A.18}$$

$$\frac{\partial E_H}{\partial \Psi_i^*(\mathbf{r})} = e^2 \int \frac{n(\mathbf{r})}{|\mathbf{r} - \mathbf{r}^{'}|} d\mathbf{r}^{'} \Psi_i(\mathbf{r}) \tag{A.19}$$

equation A.13 turns into

$$[-\frac{\hbar^2}{2m}\nabla^2 + \hat{V}_H + \hat{V}_{x-c} + \hat{V}_n]\Psi_i(\mathbf{r}) = \sum_j \lambda_{ij}\Psi_j(\mathbf{r}), \tag{A.20}$$

where we have introduced a *Hartree potential*

$$\hat{V}_H(\mathbf{r}) = e^2 \int \frac{n(\mathbf{r})}{|\mathbf{r} - \mathbf{r}'|} d\mathbf{r}' \tag{A.21}$$

and the *exchange and correlation potential*

$$\hat{V}_{x-c}(n(\mathbf{r})) = \frac{\partial E_{x-c}}{\partial n(\mathbf{r})}. \tag{A.22}$$

The Lagrange multipliers λ_{ij} are obtained by multiplying both sides of Eq.A.20 by $\Psi_k^*(\mathbf{r})$ and integrating

$$\lambda_{ij} = \int \Psi_k^*(\mathbf{r})(-\frac{\hbar^2}{2m}\nabla^2 + \hat{V}_H + \hat{V}_{x-c} + \hat{V}_{nn})\Psi_i(\mathbf{r})d\mathbf{r}. \tag{A.23}$$

For an insulator, whose states are either fully occupied or completely empty, it is always possible to make a subspace rotation in the space of Ψ (leaving the charge density invariant). We finally get the KS equations

$$(\hat{H} - \epsilon_i)\Psi_i(\mathbf{r}) = 0, \tag{A.24}$$

where $\lambda_{ij} = \delta_{ij}\epsilon_j$ and the Kohn-Sham operator for the auxiliary system is defined as

$$\begin{aligned} \hat{H} &= -\frac{\hbar^2}{2m}\nabla^2 + \hat{V}_H + \hat{V}_{x-c} + \hat{V}_{nn} \\ &= -\frac{\hbar^2}{2m}\nabla^2 + \hat{V}_n, \end{aligned} \tag{A.25}$$

and is related to the functional derivative of energy

$$\frac{\partial E}{\partial \Psi_i^*(\mathbf{r})} = \hat{H}\Psi_i(\mathbf{r}). \tag{A.26}$$

A.3 Pseudopotential Approximation

The pseudopotential approximation also known as *frozen core approximation* suggests to ignore the changes in core state. Here, the soundness of such a suggestion is presented.

Let n_c^r, n_v^r be the core and valence charge densities for the real auxiliary system and n_c^{ps}, n_v^{ps} the core and valence charge densities for the pseudo-system. As the energy $E[n_c, n_v]$ is a functional of the core and valence charge densities, let us introduce the error

$$\delta = E[n_c^r, n_v^r] - E[n_c^{ps}, n_v^{ps}]. \tag{A.27}$$

the expansion of δ around n_c^r and n_v^r yield

$$\delta \simeq \int \frac{\partial E}{\partial n_c^r}(n_c^{ps} - n_c^r)d\mathbf{r} + \frac{\partial E}{\partial n_v^r}(n_v^{ps} - n_v^r)d\mathbf{r} + \text{2nd order terms} \tag{A.28}$$

Knowing that $\partial E/\partial n_c^r$ and $\partial E/\partial n_v^r$ are constant, and that the pseudo-system meets the norm-conserving conditions (see section 1.2.1) first order terms (the most important) can be taken out of A.28 making the error δ insignificant.

A.4 Discontinuity in the Exchange-correlation Potential

The basic variational property of the density functional can be expressed by the stationary condition

$$\frac{\partial}{\partial n(\mathbf{r})}(E - \mu(\int n(\mathbf{r})d\mathbf{r} - N)) = 0, \tag{A.29}$$

where μ is a Lagrange multiplier and N an integer number. The formulation of DFT can be extended to non-integer number of particles $N + \omega$ ($\omega > 0$) via the following definition

$$E[n(\mathbf{r})] = F_{frac}[n(\mathbf{r})] + \int V(n(\mathbf{r}))n(\mathbf{r})d\mathbf{r}, \tag{A.30}$$

and

$$\begin{aligned} F_{frac}[n(\mathbf{r})] &= \min\ tr\{D(T+U)\} \\ D &= (1-\omega)|\Psi_N\rangle\langle\Psi_N| + \omega|\Psi_{N+1}\rangle\langle\Psi_{N+1}|, \end{aligned} \tag{A.31}$$

where the minimum must be sought on all density matrices D that yield the prescribed density $n(\mathbf{r})$. It is easily verified that integration of $n(\mathbf{r})$ over all space yields $N+\omega$ electrons. With this definition the variational principle, Eq. A.29, is defined for any number of electrons and yields the Euler equations

$$\frac{\delta E}{\delta n(\mathbf{r})} = \mu, \tag{A.32}$$

and that μ is really the *chemical potential*: if we call E_N the energy at the ground state for N electrons, one has

$$\mu(N) = \frac{\partial E_N}{\partial N}. \tag{A.33}$$

There is an obvious problem if we consider $\mu(N)$ a continuous function of N for all values of N. Consider two neutral isolated atoms: in general, they will have two different values for μ. As a consequence the total energy of the two atoms will be lowered by a charge transfer from the atom at a higher chemical potential to the one at lower chemical potential.
In reality there is no paradox, because the E_N curve is not continuous. If we write down explicitly $E_{N+\omega}$, we find that both energy and minimizing charge density at fractionary number of electrons are simply a linear interpolation between the respective values at the end points with N and $N+1$ electrons:

$$\begin{aligned} E_{N+\omega} &= (1-\omega)E_N + \omega E_{N+1} \\ n_{N+\omega}(\mathbf{r}) &= (1-\omega)n_N(\mathbf{r}) + \omega n_{N+1}(\mathbf{r}), \end{aligned} \tag{A.34}$$

with obvious notations. The interesting and far-reaching consequence is that there is a discontinuity of the chemical potential $\mu(N)$ and of the functional derivative $\delta E/\delta n(\mathbf{r})$ at integer N. This is an important and essential characteristic of the exact energy functional that simply reflects the discontinuity

of the energy spectrum.

Coming back to our paradox: for an atom with nuclear charge Z, ionization potential $\mathbf{I}(Z)$ and electron affinity $\mathbf{A}$(Z) in the ground state,

$$\begin{aligned} \mu(N) &= -\mathbf{I}(Z) \text{ for } N \in \ ]Z-1, Z[\\ &= -\mathbf{A}(Z) \text{ for } N \in \ ]Z, Z+1[. \end{aligned} \tag{A.35}$$

For a system of two neutral atoms with nuclear charges X and Y, in which ω electrons are transferred from the first to the second atom:

$$\begin{aligned} \mu(\omega) &= \mu(0) + \mathbf{I}(Y) - \mathbf{A}(X) \text{ for } \omega \in \ ]-1, 0[\\ &= \mu(0) + \mathbf{I}(X) - \mathbf{A}(Y) \text{ for } \omega \in \ ]0, 1[\end{aligned} \tag{A.36}$$

Since the largest $\mathbf{A}$ is still smaller than the smallest $\mathbf{I}$, the neutral ground state is stable.

Acknowledgement

when a long job is done, the straightforward acknowledgement goes to the technical and emotional supports. Prof Eric Pop and the Pop Lab from the university of Urbana-Champaign (IL, USA) as well as prof Massimo Rudan from the university of Bologna (Italy) and the Monte-Carlo Lab from the university of Modena and Reggio-Emilia are deeply thanked. My family and friends are highly credited too. A special thank to the joyful human being and selfless human having who gave me the most leverage in the most trying moment, Linda Jayne from Camargo (IL, USA).

Bibliography

[1] K. Shportko, S. Kremers, M. Woda, D. Lencer, J. Roberson and M. Wuttig, Nature Materials **7**, August (2008).

[2] B.-S. Lee, J. R. Abelson, S. G. Bishop, D.-H. Kang, B. Cheong and K.-B. Kim: *Investigation of the Optical and Electronic properties of $Ge_2Sb_2Te_5$ Phase Change Material in its Amorphous, Cubic, and Hexagonal Phases*, J. Appl. Phys. **97**, 093509 (2005).

[3] M. Ravitkumar, Pss. Srinivasan, *Phase Change Material as a Thermal Energy Storage Material for Cooling of Building*, Journal of Theoretical and Applied Information Technology (2005-2008).

[4] J. S. Sanghera et al, *Development and Infrared Applications of Chalcogenide Glass Optical Fibers*, Fiber and Integrated Optics, **19** (2000), p. 251-274

[5] A. T. Waterman, *The electrical conductivity of molydenite*, Phys. Rev. **21**, (1923) 540-549.

[6] Wang, A.: *Pulse transfer controlling devices.*, US Patent **2**, (1955) 708, 722.

[7] Kahng, D.: *Field effect semiconductor apparatus with memory involving entrapment of charge carriers.*, US Patent **3**, (1970) 500,142.

[8] Pearson, A. D., Northover, W. R., Dewald, J. F. and Peck Jr., W. F.: *Chemical, physical, and electrical properties of some unusual inorganic glasses. Adv. in Glass Tech.*, Plenum Press, New York (1962) pp. 357-365

[9] Ovshinsky, S. R.: *Reversible electrical switching phenomena in disordered structures.*, Phys. Rev. Lett. **22** (1968) 1450-1453.

[10] B. J. Kooi, Th. M. De Hosson: *Electron diffraction and high-resolution transmission electron microscopy of the high temperature crystal structures of* $Ge_xSb_2Te_{3+x}$ $x = 1, 2, 3$. *phase change material*, J. Appl. Phys. **92**, 3584 (2002).

[11] Z. Sun *et al.*: *Structure of Phase Change Materials for Data Storage*, Phys. Rev. Lett. **96**, 055507 (2006).

[12] A. Kolobov, P. Fons, A. I. Frenkel, A. L. Ankudinov, J. Tominaga, T. Uruga: *Understanding the Phase-Change Mechanism of Rewritable Optical Media*, Nature Materials **3**, October (2004).

[13] J. Akola, R. O. Jones: *Structural phase transitions on the nanoscale: The crucial pattern in the phase-change materials* $Ge_2Sb_2Te_5$ *and* $GeTe$ Phys. Rev B. **76**, 235201 (2007).

[14] S. Yamanaka et al.: *Electronic Structures and Optical Properties of* $GeTe$ $Ge_2Sb_2Te_5$, Jpn. l. Appl. Phys. **37**, p. 3327. (1998).

[15] D. Ielmini and Y. Zhang: *Evidence for Trap-limited Transport in the Subthreshold Conduction Regime of Chalcogenide Glasses* JAP **102**, 05451 (2007).

[16] D. Ielmini and Y. Zhang: *Analytical Model for Subthreshold Conduction and Threshold Switching in Chalcogenide-based Memory Devices* JAP **102**, 054517 (2007).

[17] F. Buscemi et al: *Monte Carlo Simulation of Charge Transport in Amorphous Chalcogenides*, Journal of Applied Physics **106**, 103706 (2009).

[18] M. Born, R. Oppenheimer: *On the Quantum Theory of Molecules*, Annalen der Physik **84** 457, (1927).

[19] A. Pirovano, A. Lacaita, A. Benvenuti, F. Pellizzer, and R. Bez, *Electronic Switching in Phase-Change Memories*, IEEE transactions on electron devices, **51**, 3, (2004).

[20] Thomas L. H, *The Calculation of Atomic Fields*, Proc. Cambridge Phil. Soc, **23**, 542-548 (2004).

[21] Fermi E. *Un Metodo Statistico per la Determinazione di alcune Priorieta' dell'Atomo*, Rend. Accad. Naz. Lincei, **6**, 602-607 (1927)

[22] R. M. Wentzcovitch, J. L. Martins, Price GD., *Ab initio molecular dynamics with variable cell shape: Application to MgSiO3*, Phys Rev Lett, **21**, 70 (25), 3947-3950 (1993).

[23] J. J. Kim, K. Kobayashi, E. Ikenega, M. Kobata, S. Ueda, *Electronic structure of amorphous and crystalline* $(GeTe)_{1+x}(Sb_2Te_3)_x$ *investigated using hard x-ray photoemission spectroscopy*, Phys. Rev. B. **76**, 115124 (2007).

[24] M. Born, K. Huang, *Dynamical Theory of Crystal Lattices*. Oxford University Press, Oxford, 1954.

[25] E. Schrödinger, Annalen der Physik, Vierte Folge, Band **80**, p 437 1926.

[26] D. V. Tsu, J. Vac. Sci. Technol., A **17**, 1854 (1999).

[27] *www.quantumespresso.org*

[28] R. P. Feynman, *Forces in Molecules*, Phys. Rev. **56**, 340 (1939).